Demagnetizing Effects in Active Magnetic Regenerators

by

Ozan Peksoy
B.A.Sc., Yildiz Technical University, 2000

A Thesis Submitted in Partial Fulfillment of the
Requirements for the Degree of

MASTER OF APPLIED SCIENCE

in the Department of
Mechanical Engineering

Supervisor: Dr. Andrew Rowe

Abstract

Magnetic Refrigeration (MR) relies on the ability of a magnetic substance to undergo a significant change in entropy due to the application or removal of an applied field. In Active Magnetic Regenerators (AMR) the working material tends to operate near the magnetic ordering temperature, and, because the AMR creates a temperature gradient through the bed, the local magnetic permeability can vary widely. Due to geometry and non-uniform properties, an AMR bed is subject to non-negligible demagnetizing effects which can reduce the entropy change due to an applied field.

In this thesis, a numerical model is used to examine the effects of demagnetizing fields in an AMR. Model results for single-material (Gadolinium) beds show the impacts of temperature on effective magnetization and suggest that demagnetization effects will reduce the magnetic work performed at each location in the AMR. A solution to this problem is proposed.

Table of Contents

List of Figures

List of Tables

Nomenclature

Acronyms

AMR	Active Magnetic Regenerator
MCE	Magnetocaloric Effect

Symbols

A	Cross sectional area / Surface area
B	Magnetic flux density
c	Heat capacity
H	Magnetic field intensity
I	Current
J	Current flux
M	Magnetization
M^*	Effective magnetization
m	Mass / Mass magnetization
N	Demagnetizing factor
r	Radius
S,s	Entropy, entropy per unit mass / Entropy generation
T	Temperature
W	Work
x_m	Magnetic susceptibility
α	Porosity

Subscripts

a	applied
$Curie$	Curie point
C	Cold

d	Demagnetizing
H	Hot
min	Minimum
max	Maximum
mag	Magnetic

Acknowledgements

I would like to thank my supervisor, Dr. Andrew Rowe and express my deepest appreciation for his support and guides through out my M.A. Sc. Program. This thesis would not otherwise been possible to complete. I am also grateful for the financial support provided through Natural Resources Canada, Natural Science and Engineering Research Council, and Canada Foundation for Innovation programs. I am also very thankful to my initial supervisor Dr. MacMurray Whale for his support and help. I also thank my colleagues in the IESVic group for their invaluable assistance.

Finally, I am grateful to my parents, siblings, and also my fiancée Karla for their support and encouragements.

Chapter 1

Introduction

1.1 Motivation

There are several reasons to move to fuels with lower carbon content, in particular hydrogen; climate instability due to greenhouse gas emissions being one. One of the barriers of low-carbon and carbon-free fuels is storing sufficient quantities of fuel in small volumes and with low masses. For instance, 5.8 kg hydrogen occupies 69,000 liters at standard pressure and temperature. On the other hand, the same amount of liquid hydrogen requires only 81 liters [1].

Storing hydrogen in liquid form is an option to solve the storage problem of hydrogen. Hydrogen exists in liquid form only at extremely cold temperatures (approximately 20 K). Because conventional hydrogen liquefaction technologies have efficiencies less than 35%, the real work input is significantly higher than the ideal. This leads to high power requirements and more expensive liquid hydrogen.

Therefore, a more efficient method of liquefying hydrogen is needed and refrigeration cycles using magnetic regenerators may be a solution to this problem. One of the objectives of the Cryofuels Group, a part of the Institute for Integrated Energy Systems

(IESVic) at the University of Victoria, is the development of novel devices for cryogenic cooling using magnetic cycles.

1.2 Active Magnetic Regenerator

Devices that rely on refrigeration cycles using magnetic regenerators are called Active Magnetic Regenerator (AMR) Refrigerators. Magnetic refrigeration based upon the AMR cycle has potential to be an efficient and compact means of producing refrigeration from room temperature to the cryogenic regime addressing the liquefaction problem.

A regenerator is a thermal storage medium and it is the working material in an active magnetic refrigeration cycle. Passive regenerators effectively act as insulators between a cold temperature and a hotter one. It is a porous media to allow gas to pass through. Unlike a passive regenerator, an active regenerator is thermodynamically coupled to a heat transfer fluid and produces a cooling effect. Thus, an AMR generates a temperature gradient across the AMR and acts as an insulating medium.

1.2.1 AMR Test Apparatus

The AMR Test Apparatus is a device that creates an active magnetic refrigeration cycle and allows for controlled experiments using different working materials. Various parameters can be altered to study the cycle AMR.

The AMR Test Apparatus can be divided into two main parts: the magnet as the basis of the magnetic field and the chamber. An aluminum support holds the magnet at the top of the chamber. An AMR cylinder assembly, rotated by a DC drive motor, oscillates through a clear bore located at the center of the magnet. The AMR cylinder assembly has a heat exchanger and regenerator bed on both sides. When one end is in the high field region, the other end is in a low field region. Water is used as a cooling fluid for near room temperature experiments while helium is the heat transfer fluid passing through the AMR. A chiller is used to control the temperature of the water. To avoid the heat transfer between the environment and the chamber the system is evacuated to a low pressure with a roughing and turbo pump. A drawing of the assembled AMR Test Apparatus can be seen in Figure 1.1.

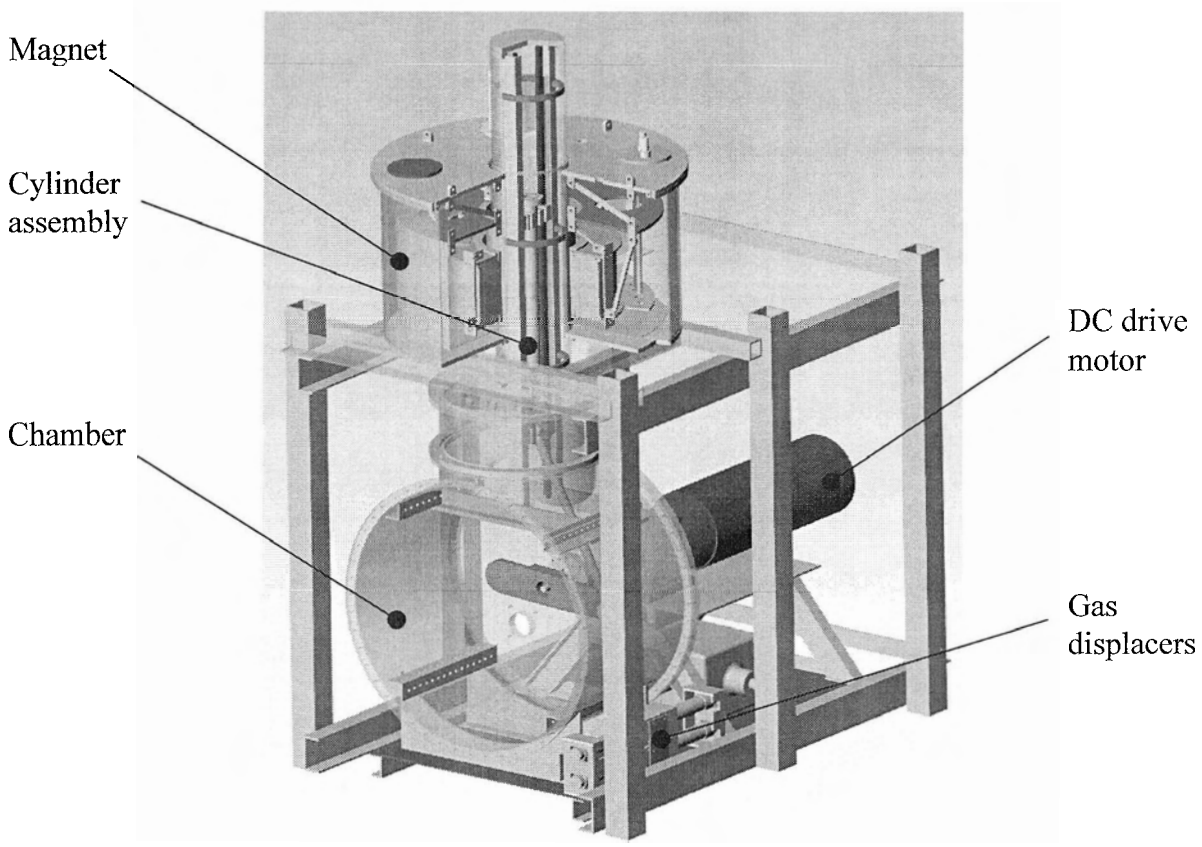

Figure 1.1: AMR Test Apparatus.

The different views of the AMR Test Apparatus in the Cryogenic Laboratory at the University of Victoria can be seen in Figure 1.2.

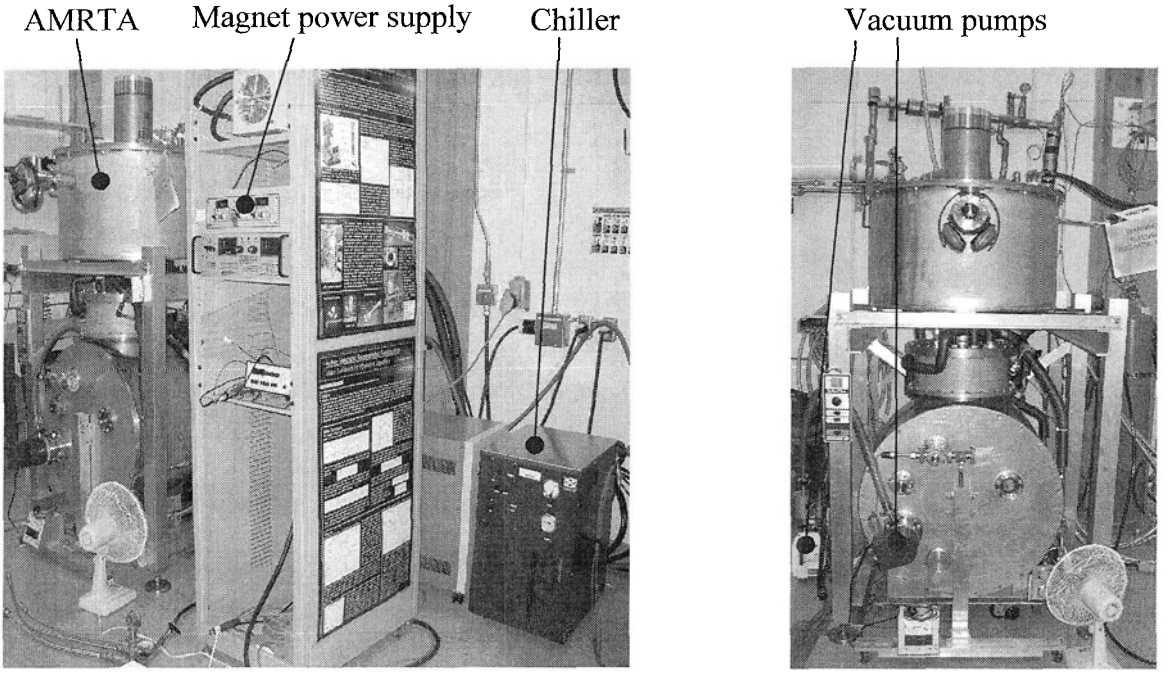

Figure 1.2: Different views of the AMR Test Apparatus.

The main parts of the AMR Test Apparatus can be described as follows:

- A magnet made of NBTi superconductor is used to create the necessary magnetic field during the experiments.
- The chamber is at the bottom of the AMR Test Apparatus. It is made of aluminum and it is the part where the AMR cylinder assembly connects to the DC drive motor.
- The AMR cylinder assembly is the main part of the test apparatus. It is made of G-10 and carries regenerators with hot heat exchangers. By sliding up and down

on guide rails, the regenerators are oscillated in and out of the high field region of the magnet. This field cycling creates the AMR cycle.

- Regenerators are on both sides of the AMR cylinder assembly and they are the devices where helium passes through. The way they are designed allows maximizing the heat transfer at the same time as to minimize the pressure drop. Regenerators are one of the most important parts of the test apparatus because these are the locations where the magnetic field affects helium. For more information the reader can refer to other studies [11,16].

1.3 Magnetic Work

The focus of this thesis is on maximizing the magnetic work performed by the regenerators. In general, the incremental magnetic work done on a magnetic material can be written in the following form:

$$\delta w_{mag} = \mathbf{B}_a \cdot d\mathbf{m} \qquad [1.1]$$

where $\mathbf{B}_a$ is the applied flux density and $\mathbf{m}$ is magnetization per unit mass.

$$\mathbf{B}_a = \mu_0 \mathbf{H}_a \qquad [1.2]$$

where $\mathbf{H}_a$ is the applied field strength and μ_0 is the permeability of free space. The total internal flux density, $\mathbf{B}$, of a magnetized body is due to the sum of total field $\mathbf{H}$ and

magnetization $\mathbf{M}$. In reality the field, $\mathbf{H}$, inside a magnetized body is not equal to the field applied to it, $\mathbf{H}_a$. Due to geometry and non-uniform properties arbitrarily shaped materials are subject to non-negligible demagnetizing effects. These demagnetizing effects are called demagnetization and are proportional to the applied field $\mathbf{H}$. The total field tends to decrease because of the demagnetization field $\mathbf{H}_d$. Easily it can be seen that the demagnetization field has a negative effect on total magnetic work:

$$\delta w_{mag} = (\mathbf{H}_a - \mathbf{H}_d + \mathbf{M}) \cdot d\mathbf{m} \qquad [1.3]$$

In order to increase the efficiency of AMRs the demagnetization effect against the magnetic work should be kept as small as possible. Many studies have been performed to examine the demagnetization effects in materials, but not in AMRs.

1.4 Relevant Work

It is well known that material shape has a significant effect on demagnetization [20]. For a material with constant permeability, it can be shown that the impact of demagnetization decrease as the slenderness of the body in the direction of the applied field increases. For this reason, when examining magnetic properties of materials, it is common practice to use long, thin samples oriented parallel to the applied field. It is then assumed that demagnetization effects are small and can be ignored.

In an ellipsoid homogeneous material where the demagnetizing field is uniform throughout the sample and proportional to the magnetization $\mathbf{M}$, the effective field in the sample can be described by

$$\mathbf{H} = \mathbf{H}_a + (\mathbf{H}_d) = \mathbf{H}_a + (-N\mathbf{M}) \qquad [1.4]$$

where N is a geometrically determined factor and $\mathbf{M}$ is the magnetization. In this case as the material is homogenous and the demagnetizing field is uniform, the demagnetizing factor N depends only on the shape of the sample and N can be calculated analytically. In the simplest case, N, is a scalar, but, in general, N is a 3×3 tensor.

Another factor that may affect the determination of the demagnetizing factor N is the possibility of small cracks or imperfections in the material. Burg and Wolf examined the demagnetizing fields in magnetic measurements for thin discs with bulk and surface imperfections [20,21]. They showed that imperfections and inhomogeneities such as pores, cracks, surface pits and scratches in the magnetized material could create demagnetizing fields. They also described different methods to calculate the effective demagnetizing factors.

In homogenous ellipsoids demagnetizing effects depend on the shape of the body and are uniform throughout the sample. In all other situations the demagnetizing fields depend on position within the body and the properties of the material. From the results for various thin disc-shaped samples it is shown that the usual approximation of a constant effective

demagnetizing factor does not exist. It is proved that the demagnetizing effects are generally field and temperature dependent. Therefore, in all magnetic measurements, in particular for high-resolution experiments, the demagnetizing correction must be estimated with accuracy [20].

A significant result of the work by Brug and Wolf [20], is that the effective demagnetizing factor N varies not only as a function of position r but also as a function of the magnetic equation of state of the material. Hence N becomes a function of field $\mathbf{H}$, temperature, T, as well as $\mathbf{r}$, ie. $N(\mathbf{r}, \mathbf{H}, T)$.

The result is that at the center of the sample the demagnetizing factor increases when the ratio of length (thickness) to radius (L/r) of the sample decreases. This variation is small but it can be significant in high-resolution measurements. Also the results show that when the susceptibility tends to zero, which means the magnetization tends to be saturated and uniform, the demagnetizing factor decreases.

Also, in the work of Brug and Wolf [20], the effect of temperature on demagnetizing factor is examined. Their results show that the demagnetizing factor increases when the temperature increases.

The AMR has some novel characteristics effecting demagnetization. Because the magnetization in an AMR bed is a function of temperature and position, the demagnetizing factor is not only due to geometry. At the Curie temperature magnetic

materials undergo a phase transition and it is in this region that AMR materials tend to operate best. When the material is behaving as ferromagnetic for lower applied fields (<2 T) there is a significant increase in magnetization. Therefore, it is expected that the demagnetizing field will be more effective in this region than a higher applied field where magnetization tends to saturate (>5 T). However, magnetization will not be saturated around the Curie temperature where the maximum magnetocaloric effect is obtained. Because of these demagnetizing fields may be a concern even for high field operations.

1.4.1 Demagnetization Field in AMRs

There have not been many reported studies of demagnetization in AMRs. In a relativley recent work Dai et al. investigated Nd-Fe-B magnets with a working material made of Gadolinium [26]. To minimize the demagnetizing field in the Gd sample and to allow the heat-exchange fluid to flow over, they used a pile of equally spaced thin Gd sheets instead of a bulk Gd geometry as shown in Figure 1.3.

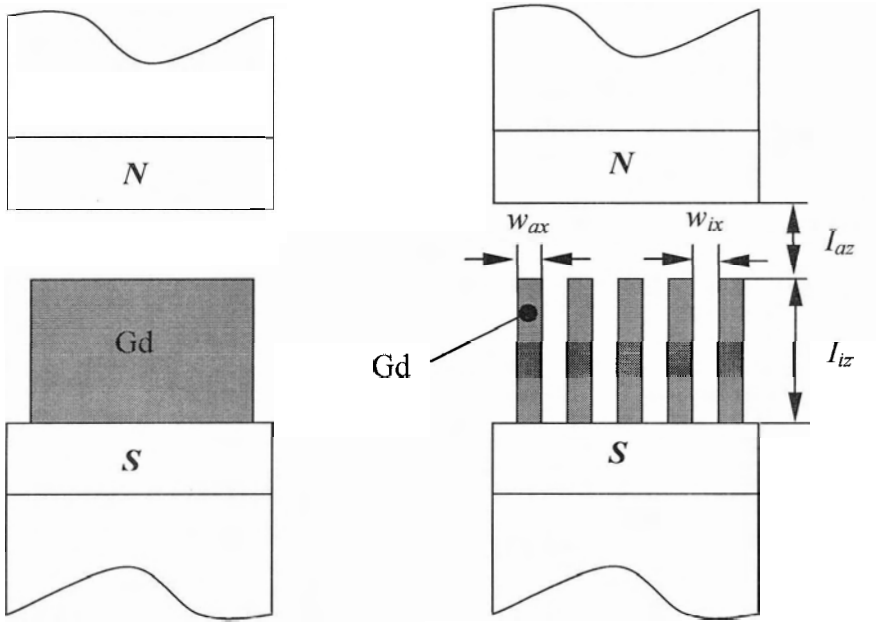

Figure 1.3: Geometry of magnet systems and a pile of Gd sheets.

They calculated the magnetic field strength, **H**, experienced by the refrigerant Gd. They estimated the average flux density in the gap by calculating the average permeability over the whole gap space as a function of the geometry of the Gd pieces, gap size and spacing (l_{az}, l_{iz}, w_{ax}, and w_{ix}). The effects of various configurations such as different applied field and different geometry ratios (L_m / L_g, l_{iz} / l_{az}, and w_{ix} / w_{ax}) were examined.

They found that the air gap (l_{az}) should be kept as small as possible to get a larger **H**, the number of magnetic pole-pieces should be increased and a moderate w_{ix} / w_{ax} ratio should be used. On the other hand, the application of some of the results is limited by the cost of the magnet.

In this thesis, as the magnetization of the ferromagnetic working body changes strongly with geometry, size and temperature, the effects of regenerator length and temperature on demagnetization are investigated.

1.5 Objective

The development of efficient and compact magnetic refrigeration devices based on an AMR cycle may offer an efficient and compact means of producing cooling at cryogenic temperatures. Magnetic refrigeration can have an impact on many areas with the production of liquid cryogens such as hydrogen being one.

Due to its complex geometry and non-uniform material properties, an AMR bed is subject to non-negligible demagnetizing effects, which can reduce the magnetic work performed by an AMR. Thus, factors that minimize demagnetization in the AMR and maximize work need to be determined.

The objective of this thesis is to investigate of demagnetization effects at different operating temperatures and at different regenerator bed sizes. A numerical model is used to examine the effects of demagnetizing fields in an AMR. In addition, a possible solution to reduce the effects of demagnetization is investigated.

Chapter 2

Demagnetization Field

2.1 Introduction

In this chapter, in order to emphasize the behavior of magnetic materials, an overview of Maxwell's magnetostatics equations is given. The magnetocaloric effect of rare earth elements, in particular Gadolinium, is discussed as is the behavior of materials under magnetic fields.

2.2 Maxwell's Theory

Maxwell's equation describes the continuity of magnetic flux through a surface. Unlike the electric flux, which leaves positive charge and enters negative charge, there are no sources or sinks from which the magnetic flux density **B** diverges. The number of magnetic lines of **B** entering into a closed system is equal to the number of magnetic lines leaving the system. Therefore, the same magnetic flux enters and leaves each closed surface and the net flux across the surface is zero.

Figure 2.1 is an example of an arbitrary surface interested by magnetic field lines. The magnetic flux density lines have no beginning or end.

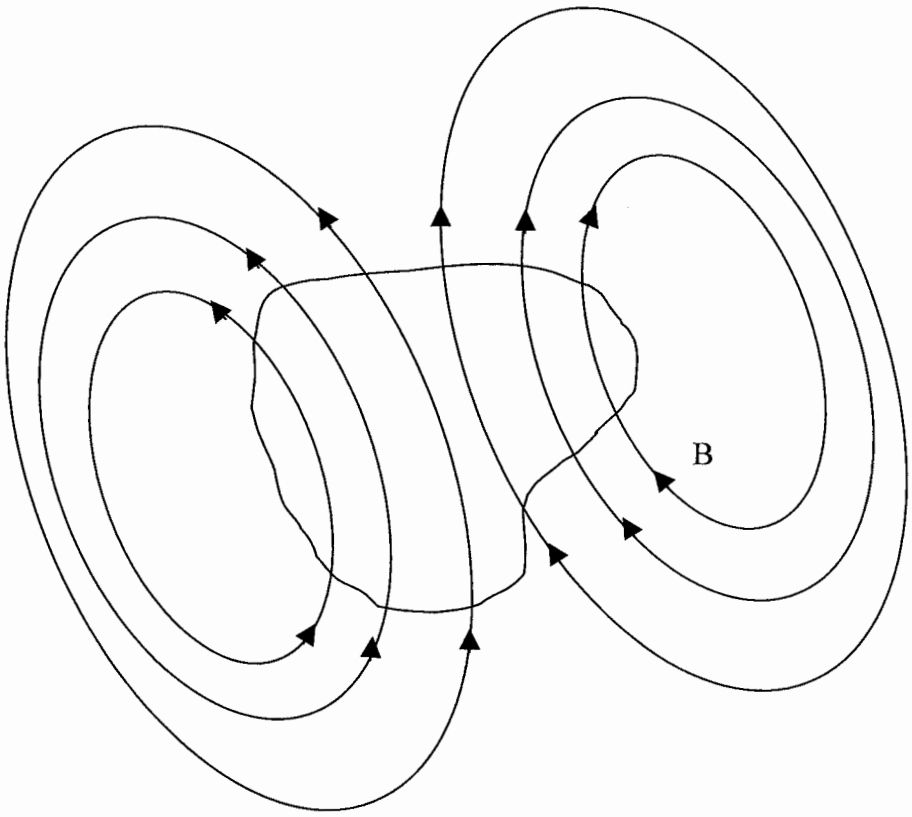

Figure 2.1: Conservation of magnetic flux.

The physical behavior is described by the following equation:

$$\nabla \cdot \mathbf{B} = 0 \qquad [2.1]$$

A magnetic field is generated by current, that is, by charge in motion. When there is no time variation of the fields, which means that the currents are steady, the curl of a magnetic field is:

$$\nabla \times \mathbf{H} = \mathbf{J} \qquad [2.2]$$

where $\mathbf{J}$ is the current density. The equation that describes the magnetic field generated by an infinitesimal current element of length dl carrying current I in the direction of the unit vector $\mathbf{i}_0$ is know as Biot-Savart Law:

$$d\mathbf{H} = \frac{Idl}{4\pi r^2}\mathbf{i}_0 \times \mathbf{r}_0 \qquad [2.3]$$

where $\mathbf{r}_0$ and $\mathbf{r}$ are, respectively, the unit vector and distance from the current element to the point at which the field is measured.

2.3 Magnetic Materials

In accordance with the Biot-Savart Law, magnetic field lines occur in the presence of a current in a body. The direction of the magnetic field lines produced by a current carrying conductor is defined by the right-hand rule. With this in mind, the field intensity and distribution produced by a coil can be determined. The concept of magnetic fields being created by current loops can be used to help explain magnetization of a material.

Because of external currents, a field $\mathbf{H}$ is produced. If a material is in the region where the field $\mathbf{H}$ exists atomic moments in the material try to align with the field. The atomic moments can be modeled as small current loops as shown in Figure 2.2. These many small current loops create an additional magnetic field that is called magnetization, $\mathbf{M}$. $\mathbf{M}$ and $\mathbf{H}$ contribute to the overall flux density in the material which is then governed by equation 2.1.

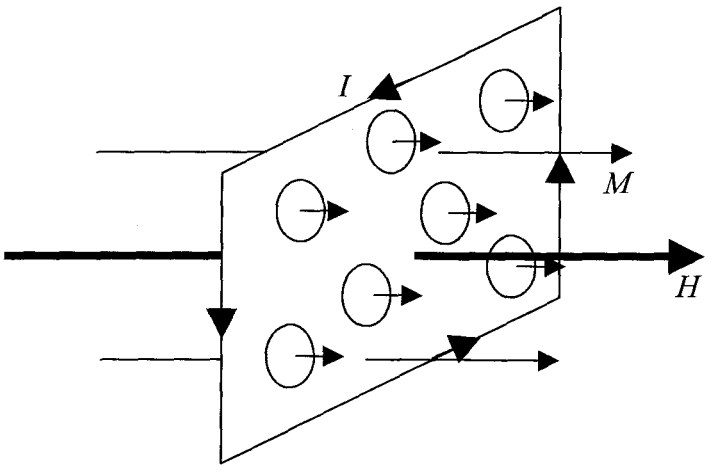

Figure 2.2: Magnetization created by a current.

The total internal flux density of a magnetized body is:

$$\mathbf{B} = \mu_0(\mathbf{H} + \mathbf{M}) \qquad [2.4]$$

where, μ_0 is the proportionality constant of vacuum. The magnetization is proportional to the local field intensity:

$$\mathbf{M} = \chi_m \mathbf{H} \qquad [2.5]$$

χ_m is called the magnetic susceptibility. Thus, equation [2.4] can be written as:

$$\mathbf{B} = \mu_0(1 + \chi_m)\mathbf{H} \qquad [2.6]$$

$$\mu \equiv \mu_0(1 + \chi_m) \qquad [2.7]$$

$$\mathbf{B} = \mu\mathbf{H} \qquad [2.8]$$

μ is the magnetic permeability of the body. In the presence of magnetized material $\mu \neq \mu_0$ because of the net magnetic moment in the material. The proportionality constant is:

$$\mu_0 = 4\pi \times 10^{-7} \text{ Wb/Am} \qquad [2.9]$$

2.4 Magnetocaloric Effects

In 1881 Warburg discovered that the temperature of some iron change reversibly with the application and removal of a magnetic field [27]. Due to a transfer of entropy from the magnetic system to the phonons in the material's crystal lattice, the temperature of the body increases because of the requirements of constant system entropy. Conversely, in adiabatic demagnetization the temperature of the body will drop returning to its original unmagnetized state in the reversible case. The phenomenon whereby magnetic materials display a characteristic, reversible temperature rise when exposed to a magnetic field is known as the magnetocaloric effect (MCE) [9].

Figure 2.3 shows the difference between a random dipole arrangement when there is no applied magnetic field (paramagnet) and the ordered dipole arrangement when there is an applied magnetic field. Molecular moments are forced to line up in the same direction because of the applied magnetic field. When the applied magnetic field is removed from

the system the molecules tend to be arranged randomly. This process is called demagnetization.

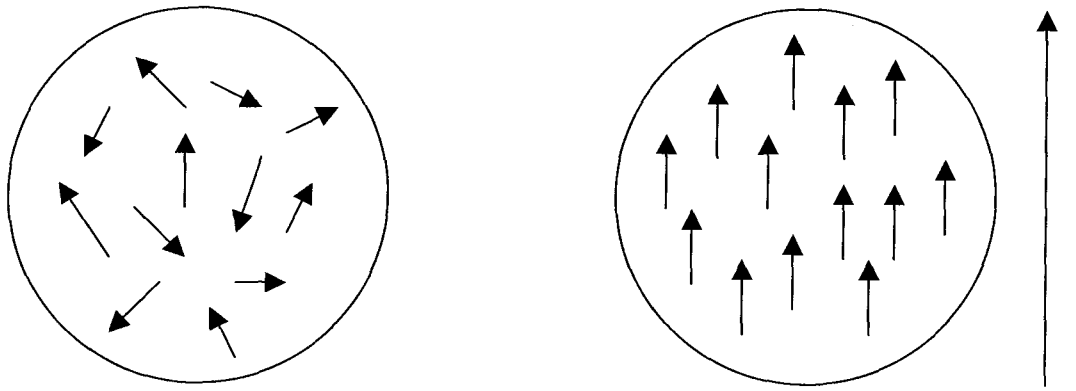

Zero field (random dipole arrangement) High field (ordered dipole arrangement)

Figure 2.3: The effect of applied field on non-interacting molecular magnetic moments.

2.4.1 Magnetocaloric Effects of Gadolinium

In most materials, the magnetocaloric effect is very small. Gadolinium, which is a well characterized rare earth element, has what can be considered a relatively high magnetocaloric effect near its transition (Curie) temperature, Figure 2.4. Below the transition temperature (293 K) Gd behaves like a ferromagnetic material and as the temperature increases it spontaneously transforms to a paramagnet.

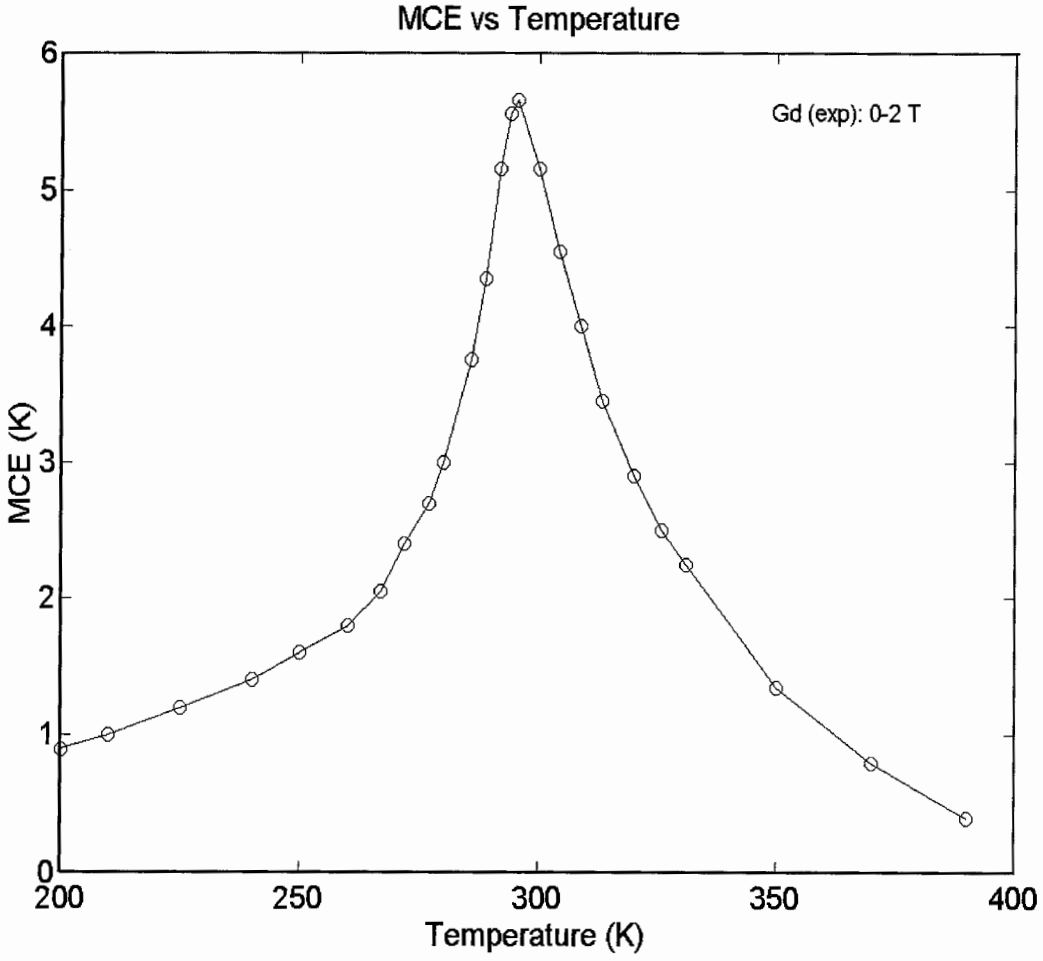

Figure 2.4: Adiabatic temperature change in Gd for 0 to 2 T [13].

Near the Curie temperature, the application of a magnetic field can create a large magnetic entropy change relative to the lattice entropy. When the temperature is moved away from the transition region, and the material is magnetically ordered or has weak magnetic interactions, an applied field has little effect and the MCE is reduced significantly.

2.4.2 Temperature Change

There are several ways to evaluate the adiabatic temperature change of magnetic materials ranging from direct temperature measurements during adiabatic applied field changes, to magnetic property measurements with data manipulation. It can be measured directly or calculated given the material's magnetization and specific heat data as a function of temperature, T, and applied magnetic field intensity, H. If the total entropy is written as a function of temperature, T, and applied field intensity, H, a differential change in entropy can be written as:

$$ds(T,H)=\left(\frac{\partial s}{\partial T}\right)_H dT+\left(\frac{\partial s}{\partial H}\right)_T dH \qquad [2.10]$$

where s is the entropy per unit mass. Using the definition of heat capacity, the above can be rewritten as:

$$ds(T,H)=\frac{c_H(T,H)}{T}dT+\left(\frac{\partial s}{\partial H}\right)_T dH \qquad [2.11]$$

If an isentropic field change is produced, the temperature change is,

$$dT=-\frac{T}{c_H(T,H)}\left(\frac{\partial s}{\partial H}\right)_T dH \qquad [2.12]$$

If Maxwell's relations for the equivalence of the second derivatives hold, the partial derivative in parentheses can be replaced to give

$$dT = -\frac{T}{c_H(T,H)}\left(\frac{\partial m(T,H)}{\partial T}\right)_H dH \qquad [2.13]$$

It can be seen that the magnetocaloric effect (temperature change) and the magnetization of magnetic materials are a strong function of temperature, T and the magnitude of the applied magnetic field, H.

2.4.3 AMR Cycle

Unlike gas cycles, or magnetic cycles, the AMR concept coupled what had been two separate processes into a single component. Instead of using a separate material as a regenerator, the AMR makes use of the refrigerant itself as the regenerator. The AMR cycle is analogous to that of a gas refrigerator where the compression and expansion processes are replaced by the magnetization and demagnetization processes (Figure 2.5). Active magnetic regenerators have two interacting materials: the regenerative magnetic working materials and the circulating heat transfer fluid. When an AMR operates these two mediums are thermodynamically coupled.

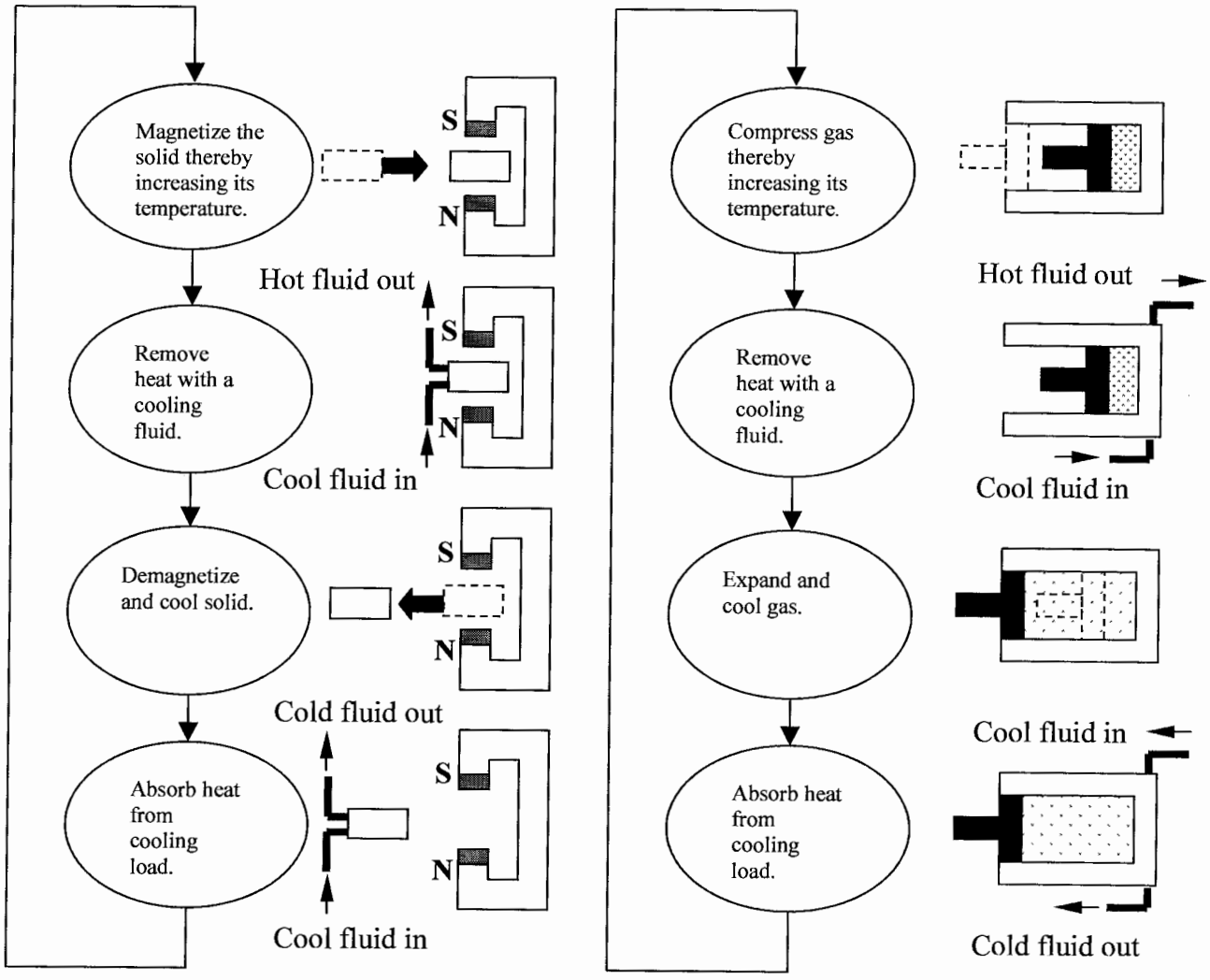

Figure 2.5: Magnetic cycle process compared with gas cycle.

An AMR cycle can be explained in four distinct steps as follows:

- The AMR is exposed to a high magnetic field in an adiabatic process, thereby causing a temperature rise at each section of the bed equal to the MCE at the local temperature.

- Heat transfer fluid is blown through the bed from the cold side to the hot side causing a small constant-field temperature change in each section.
- The bed is isentropically removed from the magnetic field thus reducing the temperature of each section by the local MCE.
- While the AMR is in a low magnetic field the fluid is blown from the hot end to the cold side of the bed, thereby warming the refrigerant.

2.5 Magnetic Refrigerants

There has been extensive research done on the selection of magnetic materials for magnetic refrigeration applications. Russian researchers have recently done a large amount of study about the magnetocaloric effects of rare earth elements [24] as have researchers at Universite de Quebec a Trois Rivières [37] and Ames Labs, Iowa [8,30].

The magnetocaloric effect (MCE) of materials is a strong non-linear function of applied magnetic field and temperature. Among all rare earth elements, Gadolinium (Gd) is the only material that orders magnetically near room temperature. The magnetic moment of Gd is quite large because of the presence of seven unpaired electrons that create a large net atomic moment. The magnetic properties of Gd have been extensively studied by Dan'kov, Tishin, Pecharsky and Gschneidner. [13].

The magnetization of Gadolinium for various magnetic fields at different temperatures is shown in Figure 2.6. From the graph it can be seen that below the Curie temperature (≈293 K), after a specific applied field (approximately 1 T) the

magnetization starts to saturate. On the other hand when the material behaves like a paramagnetic material, which means when it is above its Curie temperature, the magnetization shows almost a linear increase.

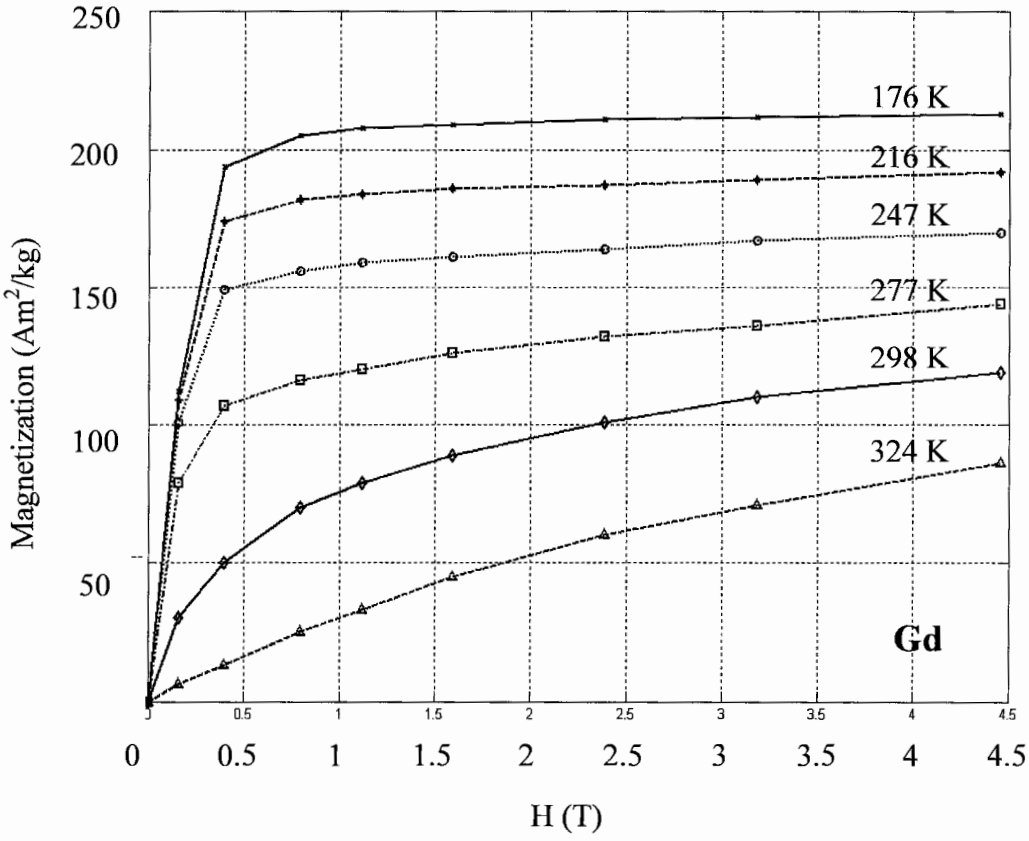

Figure 2.6: Magnetization of Gd versus magnetic fields.

The paramagnetic-ferromagnetic phase transition is a second-order magnetic phase transformation. Gd undergoes a second-order phase transition at a temperature near 293 K. Below this temperature Gd behaves like a ferromagnetic material. When the temperature is higher than the Curie temperature, Gd transforms to a paramagnetic material.

Figure 2.7 shows the qualitative magnetization curves of Gadolinium at various temperatures for three different applied fields (2.4 T, 3.6 T and 5.6 T). From the figure it can be seen that the magnetization tends to saturate below Curie temperature. Around 293 K the change in magnetization is significant compared to the other temperature regions.

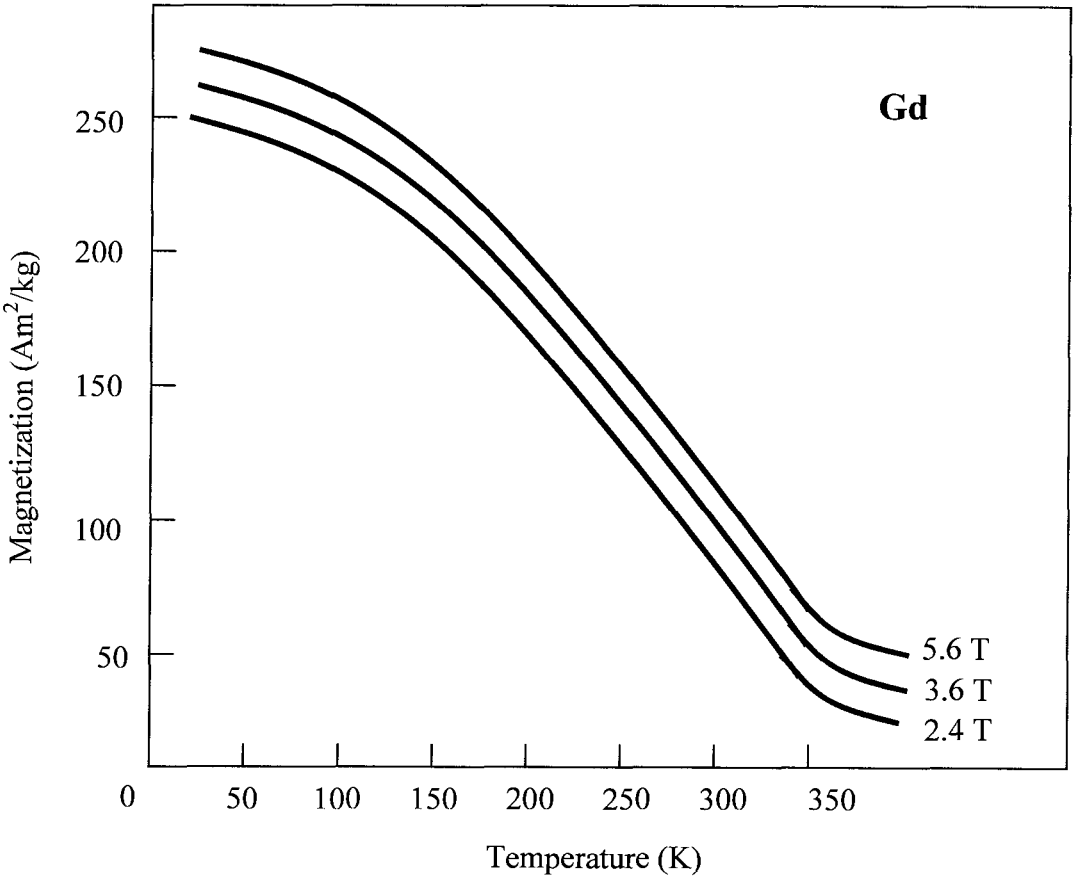

Figure 2.7: Magnetization of Gd versus temperature.

2.6 Demagnetization

A way to model a magnetized material is to picture the body as having negative and positive magnetic poles. These poles create a field in the opposite direction to the magnetization. This field is called the demagnetizing field and tends to reduce the

magnetization. In arbitrarily shaped magnetic bodies, the demagnetizing fields are not uniform. As a result, **B** and **M** will not be uniform.

In general, it is an almost impossible task to analytically calculate the demagnetization field because of the inhomogeneity of the pole and field distributions. In an ellipsoidal body that is magnetized along one of its axes, the demagnetization field can be written as:

$$\mathbf{H}_d = -N\mathbf{M} \qquad [2.14]$$

where N is the demagnetization factor along the axis.

Figure 2.8 shows a representation of the effects of demagnetization fields in a rectangular body. The demagnetization fields tend to reorient some of the magnetic domains in the body, in particular near the ends where the "magnetic poles" are.

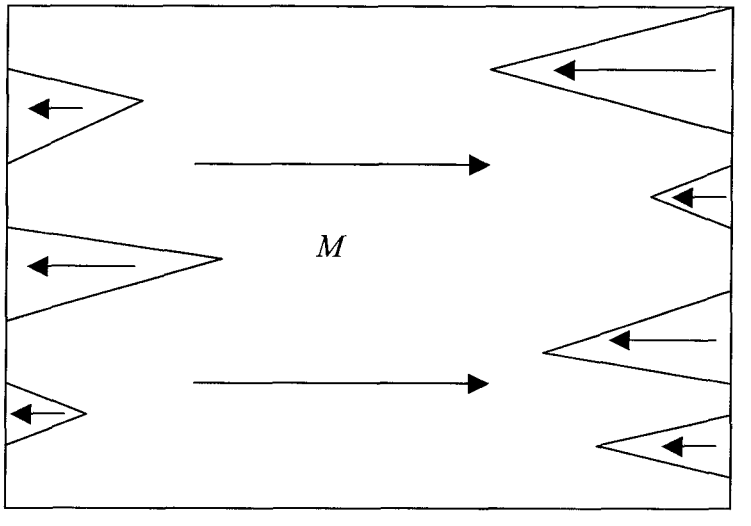

Figure 2.8: Effects of demagnetization.

Therefore, because of demagnetization effects the total magnetic field will be the sum of applied field $\mathbf{H}_a$ and demagnetization field $\mathbf{H}_d$. As $\mathbf{H}_d$ is opposite to the magnetization, it tends to decrease the total magnetic field:

$$\mathbf{H} = \mathbf{H}_a + (-\mathbf{H}_d) \qquad [2.15]$$

Chapter 3

Finite Element Modeling

3.1 Introduction

The purpose of this chapter is to describe the numerical model used to investigate the effects of demagnetization in AMRs at different temperatures and regenerator sizes. The solution domain is created to simulate the AMR bed and various cases are examined by using the Finite Element Method.

3.2 Finite Element Method (FEM)

The Finite Element Method is a powerful numerical technique to solve boundary value problems. The starting point of the FEM is the subdivision of a domain into small subdomains called elements. This process is called meshing and these elements can be of various shapes such as triangular or quadrilateral. The original body or structure is then considered as an assembly of these elements connected to a finite number of joints called nodes or nodal points. The properties of the elements are formulated and combined to obtain the properties of the entire body.

3.3 Finite Element Modeling of the Regenerator

The finite element analysis of the numerical domain was performed using ANSYS^{TM}. ANSYS^{TM} is a powerful program and it can be used for general-purpose finite element problems. The program provides a variety of elements for electromagnetic analysis. The elements that are used in simulations are "Plane 13" (2-D Coupled-Field Solid) and "Infin 9" (2-D Infinite Boundary).

"Plane 13" allows for two-dimensional magnetic, thermal and electrical field calculations with coupling between the fields. As can be seen from Figure 3.1, the element is defined by four nodes on y (Axial) and x (Radial) element coordinate system. The element has nonlinear magnetic capability for modeling B-H curves of arbitrary materials. This is important for accurate representation of magnetocaloric materials.

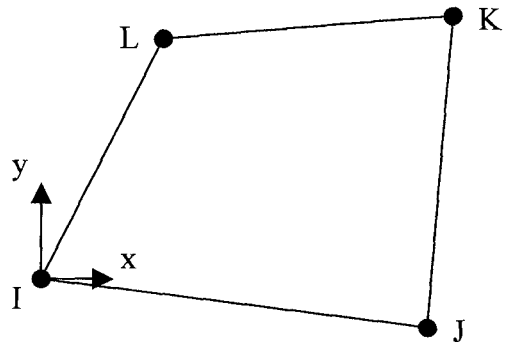

Figure 3.1: Couple field solid.

"Infin 9" is used to model an open boundary of a two-dimensional planar field problem. The element has two nodes with a magnetic vector potential or temperature degree of freedom at each node as shown in Figure 3.2. The enclosed element type can be "Plane

13". This element is needed when modeling a region of space with a current carrying element. To accurately represent the closed-loop nature of the flux lines in the region of interest, the domain needs to be large, or the boundary condition must simulate an unbounded region. "Infin 9" is the element needed to do this.

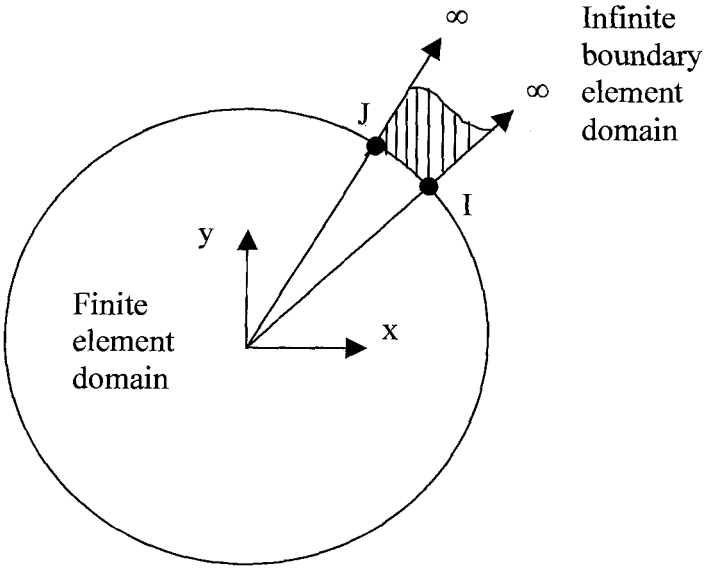

Figure 3.2: Infinite boundary element.

3.4 Model Domain

In this thesis, two different domains were investigated. The first is as shown in Figure 3.3. Here, an axis-symmetric, two-dimensional model of an AMR is shown in the situation of the AMR Test Apparatus. In the figure, the regenerator bed is positioned at the center of the magnet. And, uniform applied field in the z-direction is specified via boundary conditions. This model does not include the solenoid which allows the domain to be smaller. This leads to faster convergence.

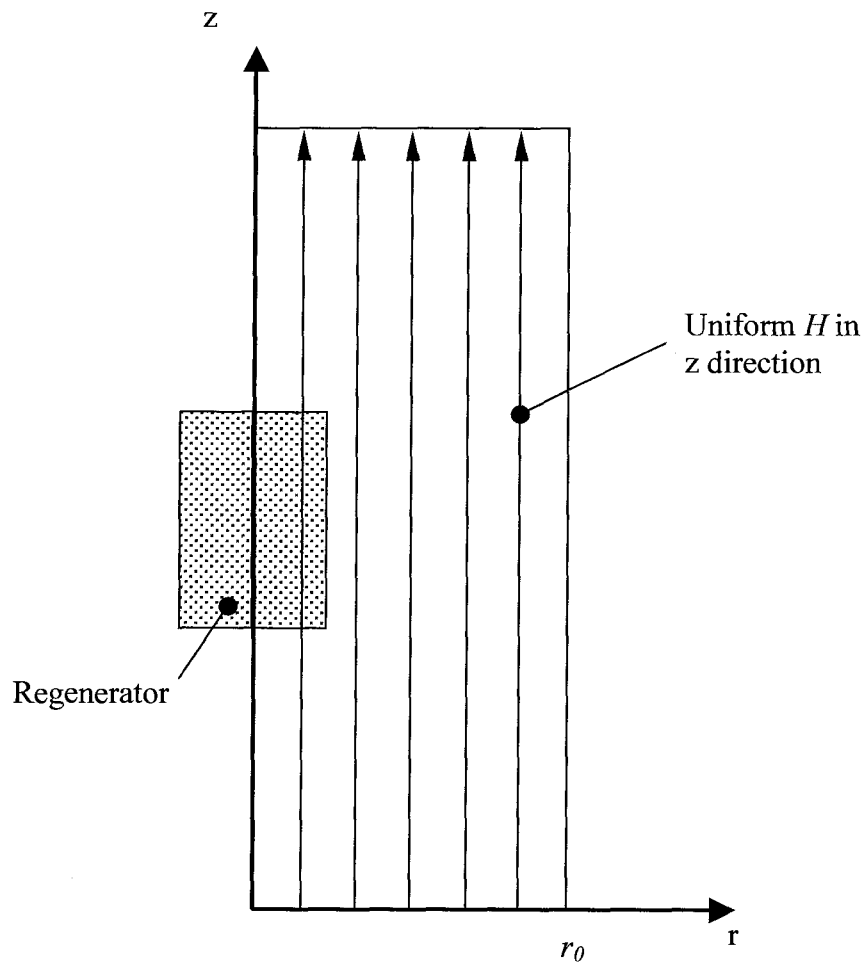

Figure 3.3: Finite element model of the AMR bed.

A second model is shown in Figure 3.4. This domain includes the solenoid windings and more accurately simulates the shape of the actual field lines. The problem with this model is that the domain is large and the area of interest is a relatively small portion.

In this model, the "Infin 9" element is used on the boundaries not on the symmetry axis, and the field strength, H, is set by adjusting the current density in the region representing

the coil. For an applied field of $\mu_0 H = 2T$, at (r=0, z=0) the current density is set at 76×10^6 A/m^2.

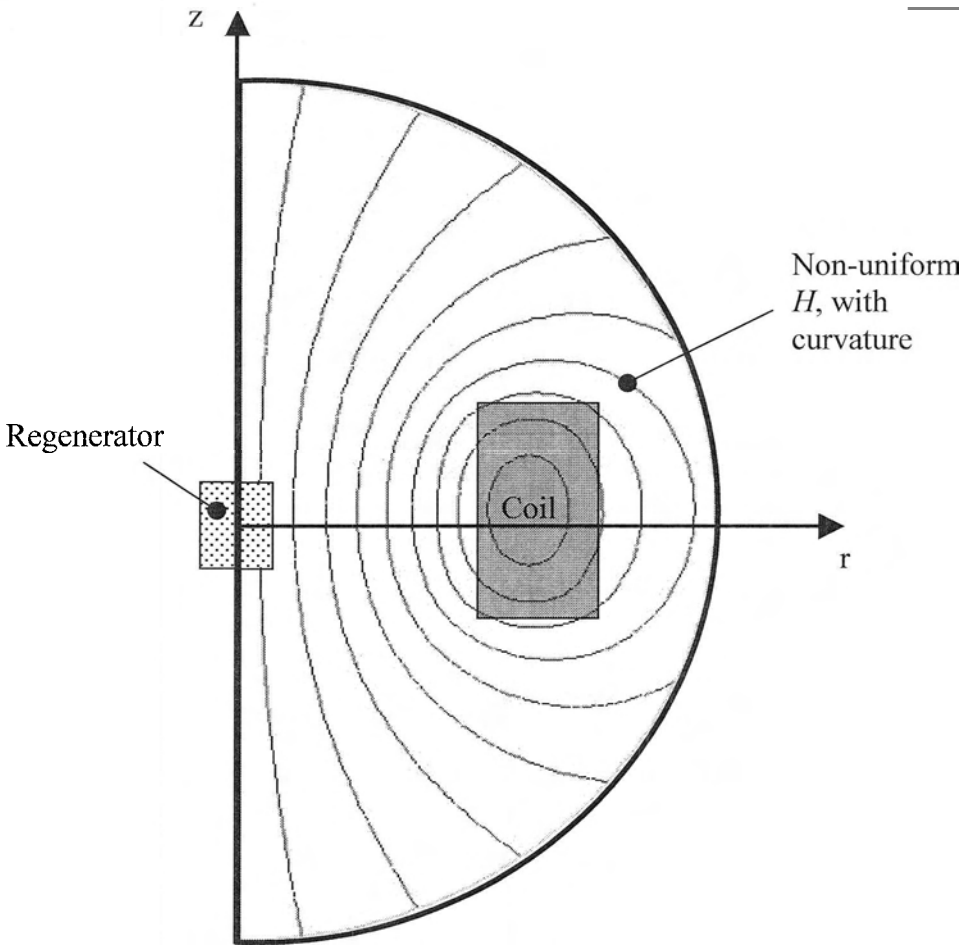

Figure 3.4: Finite element model of the AMR bed with solenoid.

This second model was needed to determine if the curvature of the field lines in the region where the AMR is located have a significant effect on demagnetization. This is discussed later, but the difference between the two models can be shown by the field lines, **H**, that are applied.

Like the regenerators tested in AMR, the modeled bed has a diameter of 25 mm and is filled with porous magnetic material. For various temperatures, different B-H tables of Gadolinium are stored as text files. These text files are used in the software to input material properties. To find the exact B-H table values for specific temperatures a simple interpolation algorithm is written in Matlab™.

3.4.1 Porosity

One of the difficulties with modeling the magnetization of an AMR is a result of the porosity. The domain in the model representing the regenerator assumes that the magnetization is continuous over the area. In reality, the volume of the bed can contain on the order of 50% magnetocaloric material and 50% helium gas. To account for this, it is assumed that the magnetic moment per unit volume can be scaled by porosity to represent the position dependent magnetization. Thus, the porosity of the AMR is assumed to be 0.55 and the magnetization per unit volume, M, is scaled to account for porosity, α. Therefore, a scaling factor is used to define an effective magnetization, M^* as follows:

$$M^* = (1-\alpha)M \qquad [3.1]$$

$$\mathbf{B} = \mu_0(\mathbf{H} + \mathbf{M}^*) \qquad [3.2]$$

3.4.2 Mesh Generation

Before the boundary conditions are set, the mesh generation of the computational domain was created. The domain has 75 mm by 250 mm dimensions. Quadratic element with 2.5 mm length is used to mesh the domain. In order to achieve more accurate result on the regenerator bed, a finer mesh is applied to this area as shown in Figure 3.5. Therefore, over 3000 elements are obtained.

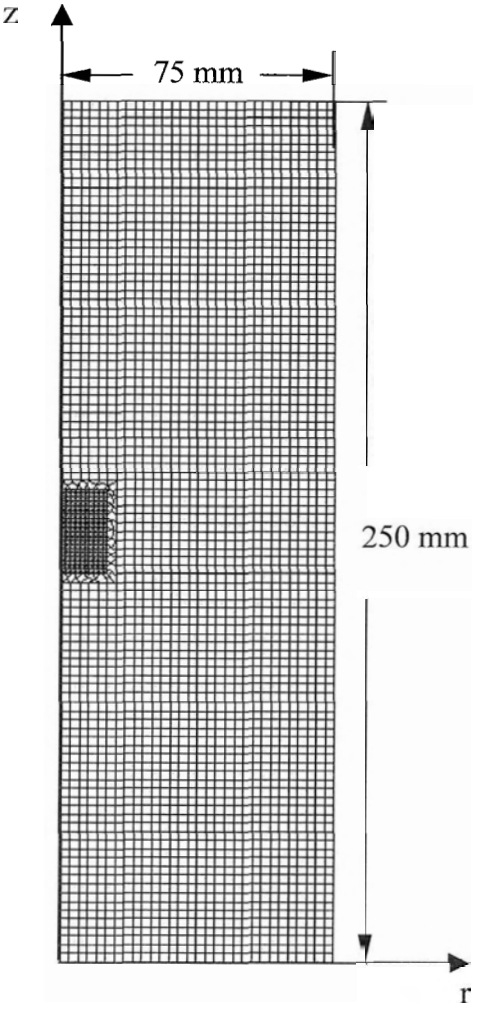

Figure 3.5: Mesh generation of the computational domain.

The advantage of having a finer mesh on the regenerator bed is to save from CPU time. The CPU time of the simulations is approximately 120 sec. To see if the mesh size has

any effects on the results, another simulation was performed with finer mesh. The change in the results is negligible and, therefore, the mesh size is deemed appropriate.

3.4.3 Boundary Conditions

It is well known that the magnetic flux lines **B** leaving and entering a closed system are equal and, the divergence of magnetic lines **B** is equal to zero. Because the divergence of any curl is zero, a magnetic vector potential can be defined such that [12],

$$\mathbf{B} = \nabla \times \mathbf{A} \qquad [3.3]$$

$$\nabla \cdot \mathbf{B} = \nabla \cdot (\nabla \times \mathbf{A}) \qquad [3.4]$$

Using the curl of **A**, the three components of flux **B** can be written,

$$B_r = (\nabla \times A)_r = \frac{1}{r}\frac{\partial A_z}{\partial \phi} - \frac{\partial A_\phi}{\partial z} \qquad [3.5]$$

$$B_\phi = (\nabla \times A)_\phi = \frac{\partial A_r}{\partial z} - \frac{\partial A_z}{\partial r} \qquad [3.6]$$

$$B_z = (\nabla \times A)_z = \frac{1}{r}\frac{\partial}{\partial r}(rA_\phi) - \frac{1}{r}\frac{\partial A_r}{\partial \phi} \qquad [3.7]$$

For symmetry, $B_\phi = 0$, and in the circumferential direction,

$$\frac{\partial A_z}{\partial \phi} = 0 \qquad [3.8]$$

$$\frac{\partial A_r}{\partial \phi} = 0 \qquad [3.9]$$

Thus, B_r and B_z are determined by the vector potential relations,

$$B_r = -\frac{\partial A_\phi}{\partial z} \qquad [3.10]$$

$$B_z = \frac{1}{r}\frac{\partial}{\partial r}\left(rA_\phi\right) \qquad [3.11]$$

The advantage of using magnetic vector potential for this 2-D problem is that only a single component of $\mathbf{A}$ is solved for, A_ϕ. Knowing A_ϕ over the domain, B_r and B_z can be determined by differentiation.

The vector potential $\mathbf{A}$ has three components corresponding to the directions of the cylindrical coordinates (r, z and ϕ). For the model assuming a uniform applied field in the z direction, the flux at the boundaries is only in the z direction. Hence, the boundary condition for $\mathbf{A}$ on $r=r_0$ in a cylindrical coordinate system can be determined as follows where $\mathbf{A}$ represents A_ϕ :

$$B_z = \frac{1}{r}\frac{\partial(rA)}{\partial r} \qquad [3.12]$$

$$(rA)_{r_0} - (rA)_{r=0} = \int_0^{r_0} rB_z dr \qquad [3.13]$$

because the applied field is uniform and constant,

$$(rA)_{r_0} = B_z \int_0^{r_0} r dr = \frac{B_z r_0^2}{2} \qquad [3.14]$$

$$(rA)_{r_0} = \frac{Br_0^2}{2} \qquad [3.15]$$

therefore, the boundary condition for $A(r=r_0)$ is,

$$(A)_{r_0} = \frac{Br_0}{2} \qquad [3.16]$$

On the axis of symmetry, $r=0$, the vector potential $\mathbf{A}$ is set equal to zero:

$$(A)_0 = 0 \qquad [3.17]$$

Both of these conditions effectively state that no flux lines cross the boundaries. For the top and bottom surfaces, the boundary conditions are:

$$\frac{\partial A}{\partial z} = 0 \qquad [3.18]$$

signifying that the flux lines are normal to the surface.

3.5 AMR Operating Regimes

The final piece of information needed to solve for the magnetization, is the constitutive relation for M as a function of H through the AMR. Because $M(H)$ is a function of temperature, a temperature profile through the AMR must be specified. The possible operating regimes of an AMR in terms of temperature can be described in three regimes:

1. $T_{Curie} > T$
2. $T_H > T_{Curie} > T_C$
3. $T > T_{Curie}$

where T_{Curie} is the Curie temperature, T_H is the average temperature of the refrigerant material at the hot end of the AMR and T_C is the average temperature of the refrigerant at the cold end of the bed.

For all situations a temperature gradient exists across the regenerator bed. In the first case, the temperature of the material at all locations in the AMR is less than the Curie temperature. In the second case, the cold end of the AMR is below and the hot end of the AMR is above the Curie temperature. These two conditions are common for single material AMRs. In the last case the material in the regenerator is operating above the

Curie temperature. This situation can occur during start-up, when the AMR is cooling down, or in a layered AMR during transient or steady-state operation.

Because the temperature of the regenerator material has a significant effect on magnetization, these three operating regimes are investigated in the simulations. Results of AMRs with various aspect ratios, as well as temperatures, are also investigated. One of the key questions still needing to be answered is how much material is needed for effective AMRs. Thus, aspect ratio is the variable used to examine this.

Chapter 4

Numerical Results

4.1 Introduction

In this chapter, the demagnetization in AMR beds for a single material (Gd) is investigated. Several simulations are performed at different temperatures and regenerator sizes in order to determine the effects of demagnetization fields on magnetization. Because this can lead to reduced cycle work, it is important that demagnetizing effects be minimized. Thus, a solution to the problem is proposed and investigated using the FEM model.

4.2 Results

In each simulation, the local field, $\mathbf{H}$, is determined along the center of the AMR and the data are written to a file. The local field (that results when there are no demagnetizing effects) is then used to determine the local magnetization, $\mathbf{M}$. The magnetization using the applied field, $\mathbf{H}_a$ can also be calculated. This value is labeled $\mathbf{M}_0$. The ratio of these two values is defined as the relative magnetization as follows:

$$\frac{M}{M_0} \equiv \frac{M(H,T)}{M(H_a,T)} \qquad [4.1]$$

If there are no demagnetization effects, the relative magnetization is equal to 1.

4.2.1 Results for Temperature Variation

For the first simulations, the effect of uniform temperature on demagnetization is examined. The applied field is 2 T and the regenerator diameter is set at 25 mm. The regenerator length is kept constant at 25 mm. The simulations are performed for three different operating regimes such as, below Curie temperature, (277 K), above Curie temperature, (305 K) and near the transition temperature, (298 K). These cases are listed as 1 a, b and c in Table 4.1. These simulations provide insights into material behavior when an AMR test is first started and the bed is at uniform initial temperature.

Conditions:		Applied Field, B_a = 2 T Regenerator Diameter = 25 mm Material Magnetization Curve, Gd (Curie Temp = 293 K)		
Case		Description	Temperature (K)	Length (mm)
1	a.	Above Curie point	305	25
	b.	Near Curie Point	298	25
	c.	Below Curie point	277	25

Table 4.1: Geometry, material properties, and imposed conditions for temperature variation.

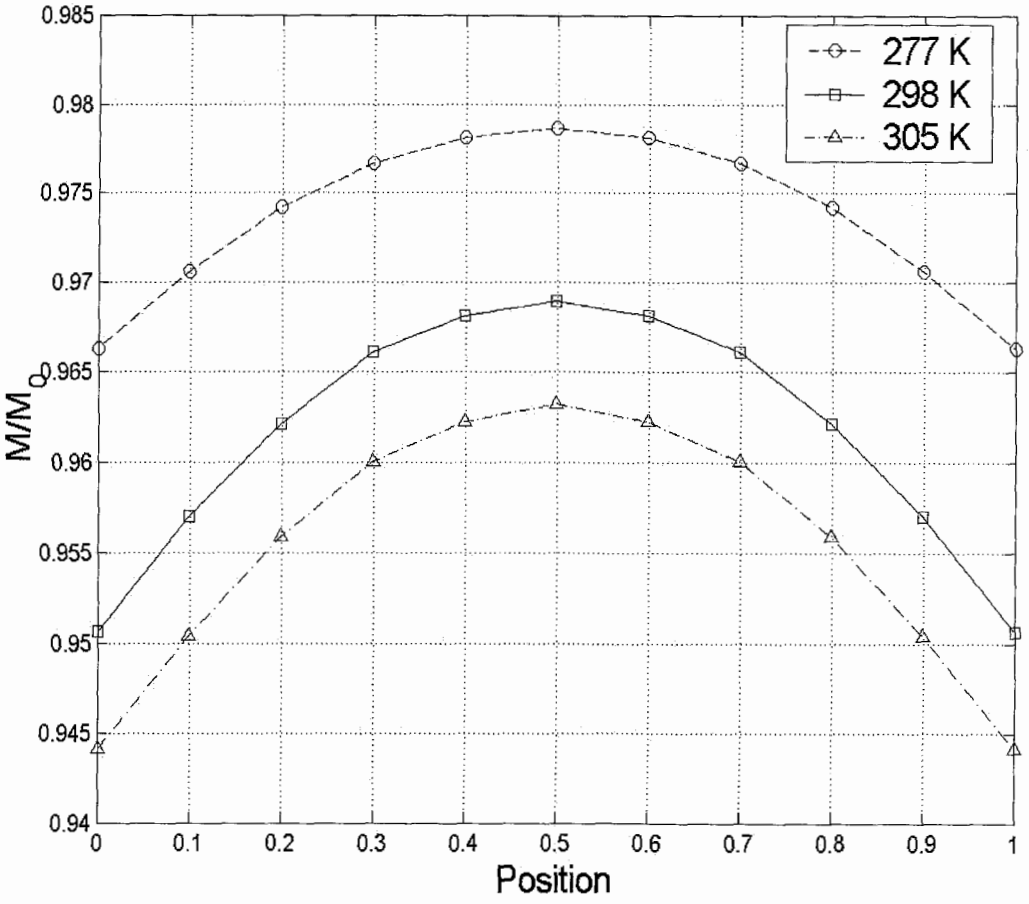

Figure 4.1: Relative magnetization at various temperatures.

The results of simulating an AMR with a fixed length of 25 mm and with uniform, but varying temperatures are shown in Figure 4.1. The relative magnetization plotted for the centre of the AMR. As the temperature of the refrigerant goes from a point below Curie temperature to a temperature greater than Curie point, the relative magnetization decreases. It can also be seen that demagnetization effects are greatest near the ends of the regenerator. This is to be expected since the permeability of what is effectively free space outside the AMR is much lower than within the regenerator. Thus, it is expected

that an AMR operating near or above the phase transition region will not perform as much work as expected and will be less effective in pumping heat.

4.2.2 Results for Length Variation

The second case examined is the effect of regenerator aspect ratio on demagnetization. For 2 T applied field and 25 mm regenerator diameter three aspect ratios are chosen (0.5, 1 and 1.5). The temperature is constant at approximately 5 K above the Curie temperature. Geometry, material properties, and imposed conditions are summarized in Table 4.2.

Conditions:		Applied Field, B_a = 2 T Regenerator Diameter = 25 mm Material Magnetization Curve, Gd (Curie Temp = 293 K)		
Case		Description	Temperature (K)	Length (mm)
2	a.	Aspect Ratio = 0.5 (L/D)	298	12.5
	b.	Aspect Ratio = 1	298	25
	c.	Aspect Ratio = 1.5	298	37.5

Table 4.2: Geometry, material properties, and imposed conditions for length variation.

Figure 4.2 shows the model results for the above cases. At 298 K, the magnetization versus applied field curve lies in between that of a prototypical ferromagnet and a paramagnet. As expected, for a fixed temperature the demagnetizing effect is strongest near the ends of the regenerator and tends to increase as the length is reduced from 37.5 mm to 12.5 mm. The effect of aspect ratio is important in understanding layered regenerators, where multiple materials may be stacked in an AMR. A thin layer is

desirable so that a minimum amount of material is used. However, as can be seen in Figure 4.2, thinner layers suffer from larger demagnetizing effects.

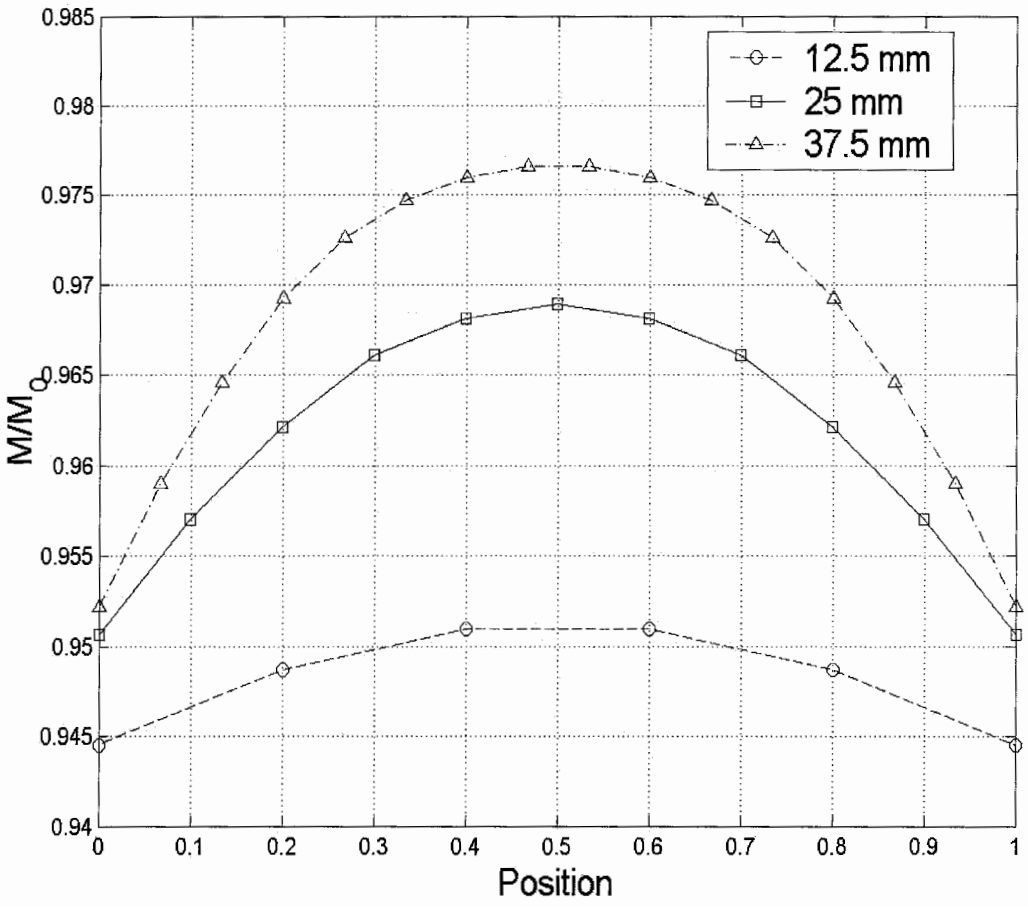

Figure 4.2: Relative magnetization at various regenerator lengths.

4.2.3 Impacts of Temperature Gradient

In reality, the regenerator temperature is not constant or uniform. At steady-state, a temperature distribution exists through the bed. To examine this, simulations with the bottom of the regenerator bed assumed to be 285 K and the top 302 K are performed. The temperatures inside the AMR are assumed to be linearly distributed from 285 K to 302 K

as shown in Figure 4.3. The simulations are performed for three different aspect ratios (0.5, 1 and 1.5) as shown in Table 4.3.

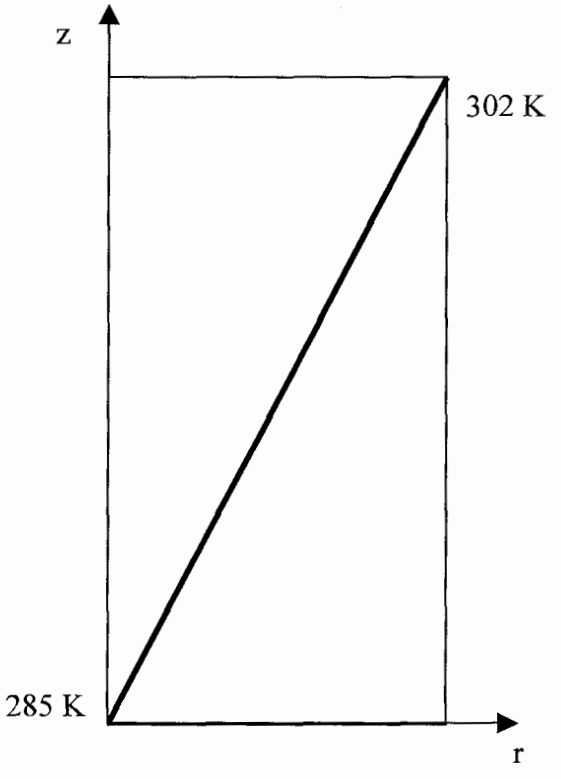

Figure 4.3: Temperature distribution through the regenerator bed.

Conditions:		Applied Field, B_a = 2 T Regenerator Diameter = 25 mm Material Magnetization Curve, Gd (Curie Temp = 293 K)		
Case		Description	Temperature (K)	Length (mm)
3	a.	Aspect Ratio = 0.5, T varies	285-302	12.5
	b.	Aspect Ratio = 1, T varies	285-302	25
	c.	Aspect Ratio = 1.5, T varies	285-302	37.5

Table 4.3: Geometry, material properties, and imposed conditions for temperature span.

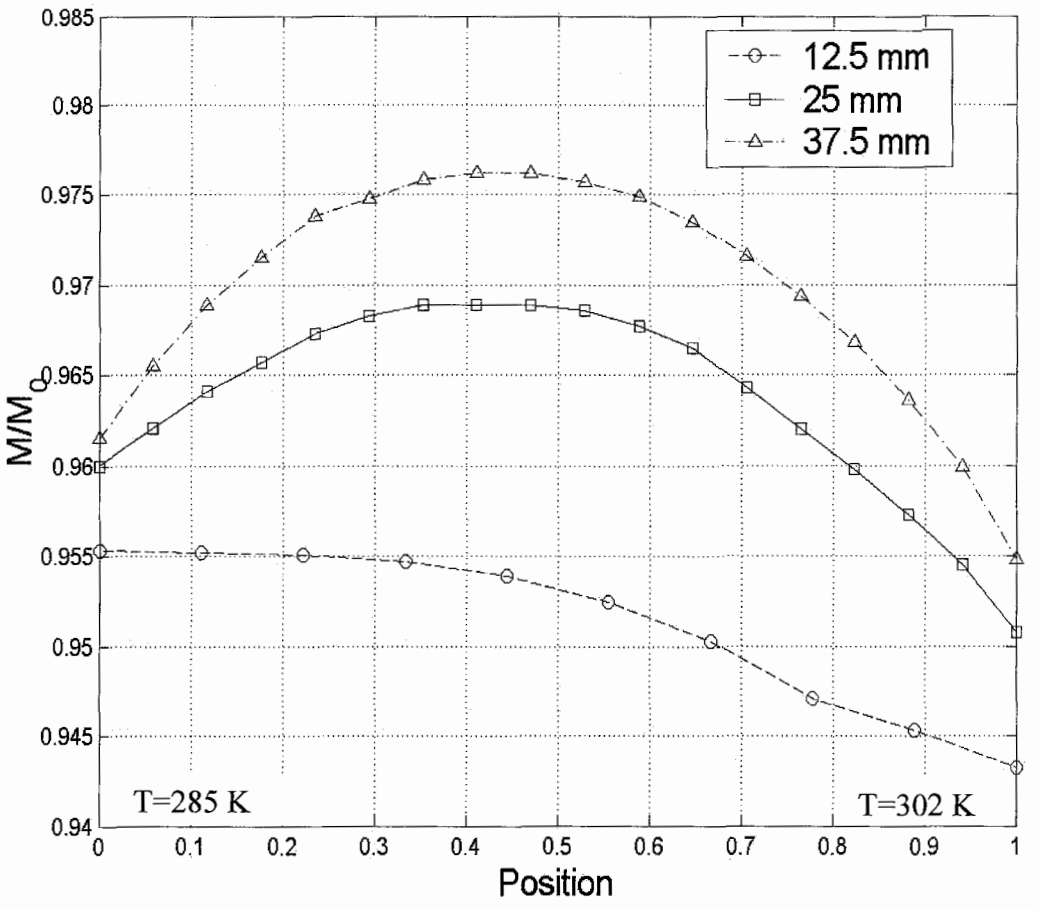

Figure 4.4: Relative magnetization for temperature span at various regenerator lengths.

In Figure 4.4, the cold end of the AMR is at position zero on the length coordinate while the hot end is at 1. For the specified temperature profile and with Gd, the cold end is in the ferromagnetic regime while the hot end is near paramagnetic. Similar to the results of Case 1, the sections that are paramagnetic show a larger response to demagnetizing fields. Also shown is the impact of aspect ratio. Again, a longer bed has a larger relative magnetization at all positions along the regenerator centerline. This simulation most closely represents an operating AMR. Experimental results [29] have shown that the

largest temperature spans occur when the hot temperature and cold temperature straddle the Curie temperature. However, the experimental temperature span is not as large as models predict. Demagnetizing effects may be a reason for this.

4.3 Flux Shimming

From the previous results it can be seen that the demagnetization effects tend to decrease the magnetization and will impact magnetic work. The reduction in magnetization for a given applied field due to geometry and material properties has a negative impact on magnetic work. For single material AMRs at lower applied fields (<2 T), when the material is most susceptible to demagnetization, it should be possible to counteract the demagnetizing effect to some degree by the careful use of other magnetic materials. A material with high magnetic permeability will tend to channel the flux lines and can increase local field strengths near the material. The model results have shown that the magnetization is most affected near the boundaries of the AMR. Therefore, putting passive magnetic material near the boundaries should help contain the magnetic flux and reduce magnetization. The use of passive materials to shape the magnetic field is called "flux shimming".

The AMR Test Apparatus can accommodate regenerators of various lengths and allows for the addition of spacers on either end of the regenerator beds. To counteract the effects of demagnetization, the use of passive ferromagnetic material disks on either end of the regenerators is proposed. Figure 4.5 shows how this idea is expected to work. Two flux

shims are shown on either side of the regenerator and the resulting field distribution near the ends of the AMR is compared to the situation where there are no shims.

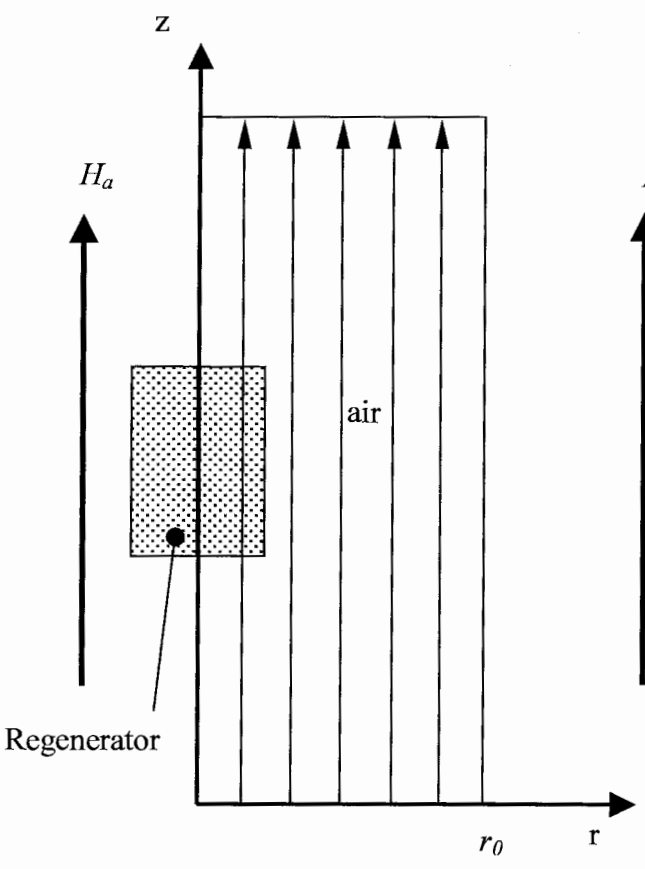

Figure 4.5.a: Flux without shimming.

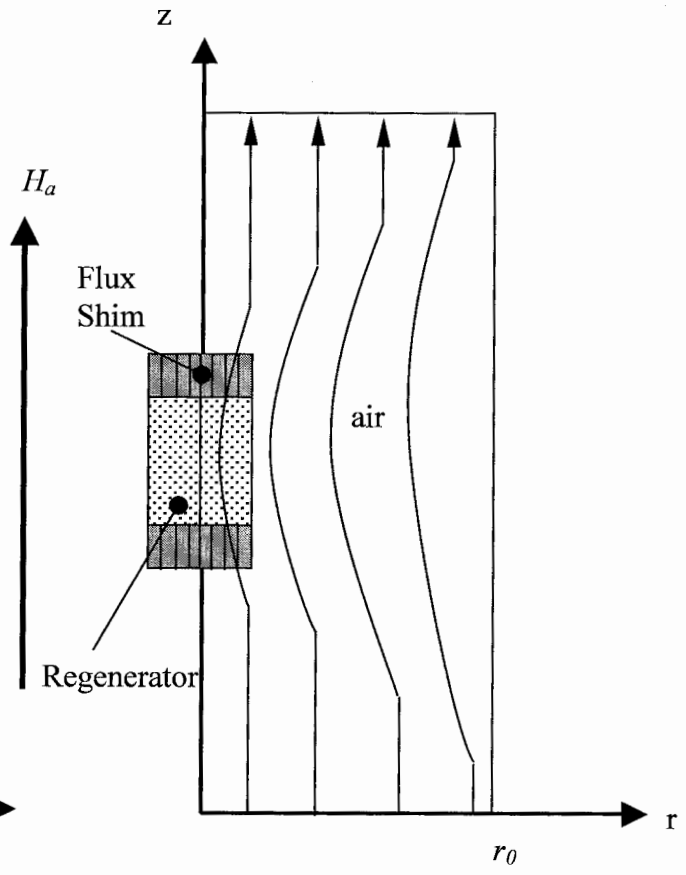

Figure 4.5.b: Flux with shimming.

4.3.1 Iron Inserts

A material such as soft iron, with low hysteresis and high saturation fields, may be able to increase the effective field seen by the regenerators, in particular near the ends. To examine flux shimming, porous steel disks have been fabricated to be placed on either end of a regenerator. Disks approximately 12 mm in length with perforations around the

circumference allow fluid to oscillate through the AMRs while keeping as much material as possible near the center to focus the field, Figure 4.6.

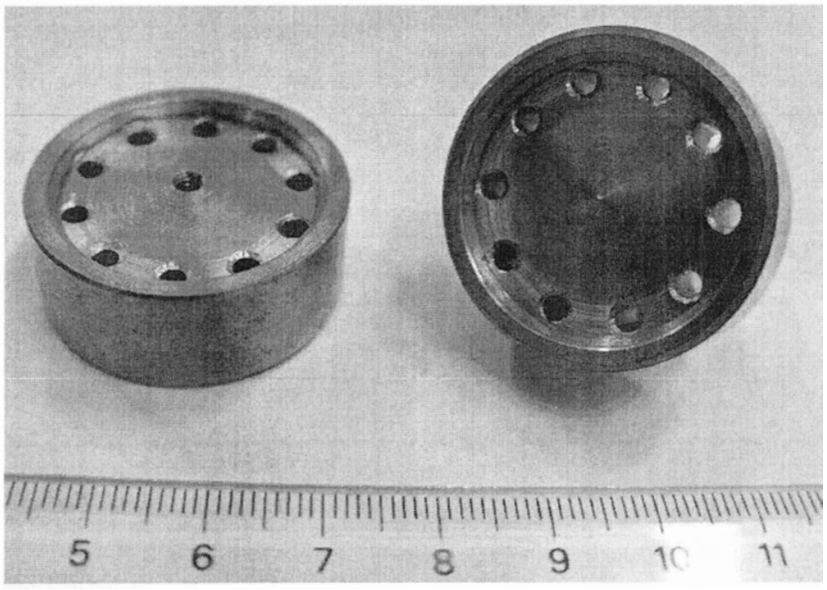

Figure 4.6: Flux shims.

The shims are made of 1018 steel and the B-H curve of the material can be seen in Figure 4.7. It can be seen that for lower fields **B** increases significantly and tends to saturate for higher applied fields standard behavior for a ferromagnetic material. The technical drawing of the pieces can be found in Appendix A.

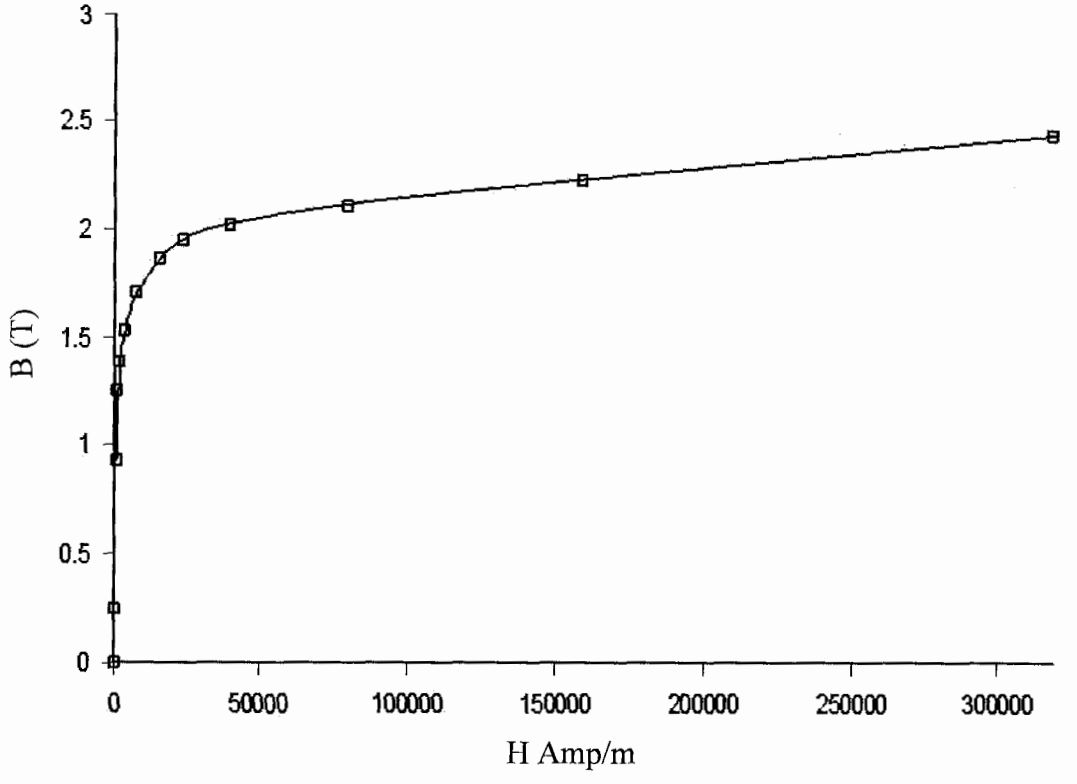

Figure 4.7: B-H curve of Steel-1018.

4.3.2 Numerical Results With Flux Shimming

Prior to experimentally examining the effects of the flux shims on the performance of the AMRs, their use was modeled in Ansys™. A subdomain for the shims is created and the magnetic properties for 1018 steel are used to describe the subdomain B-H response. Three different regenerator lengths (12.5 mm, 25 mm and 37.5 mm) with a temperature span (285 K – 302 K) are examined and listed as Case 4 in Table 4.4.

Conditions:		Applied Field, B_a = 2 T Regenerator Diameter = 25 mm Material Magnetization Curve, Gd (Curie Temp = 293 K)		
Case		Description	Temperature (K)	Length (mm)
4	a.	AR = 0.5, Flux Shim	285-302	12.5
	b.	AR = 1, Flux Shim	285-302	25
	c.	AR = 1.5, Flux Shim	285-302	37.5

Table 4.4: Geometry, material properties, and imposed conditions for flux shimming.

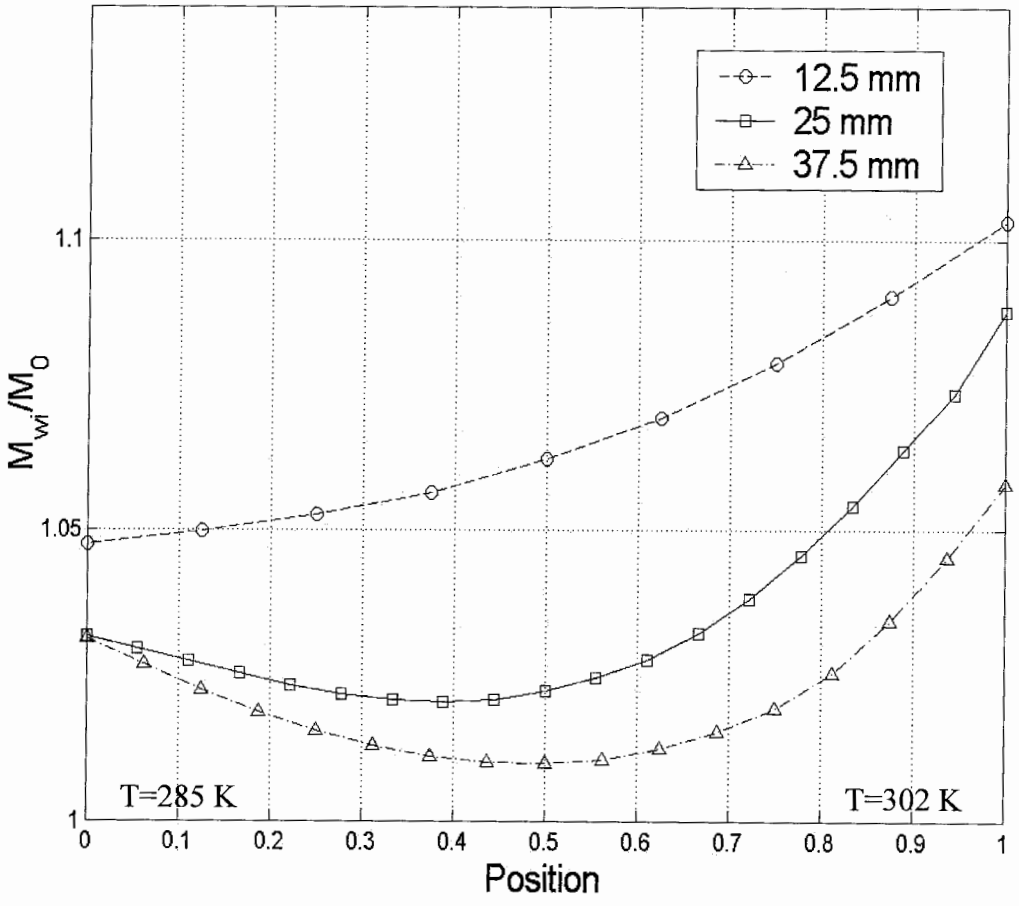

Figure 4.8: Relative magnetization for flux shimming.

The impacts of using flux shimming are shown in Figure 4.8. The results indicate that the shims reduce the demagnetization effect through the AMR on the centerline. The increase in magnetization is most significant for the shorter regenerators and for the material that is near and above the Curie temperature.

While the simulations have only shown regenerators using single materials, one can see that a multi-layer bed may have similar features to the above simulation with the flux shims. In a layered regenerator, one of the layers may be operating below its Curie temperature (being ferromagnetic) and, thereby, acts like a flux shim on an adjacent material that is above its Curie point (paramagnetic). This is a subject of ongoing investigation. The results that are shown above are for the axis of a cylindrical AMR. The areas away from the center of the regenerator are much more seriously affected.

4.4 Realistic Field Distribution

In the AMR Test Apparatus, the field generated by the solenoid is not perfectly uniform in the area where the regenerators are. To see if this effect is significant, a more realistic model was created including the coil. This is shown in Figure 4.9. The infinite boundary element, Infin 9, is applied on the curve boundary of the domain and solenoid flux lines are obtained due to the coil current.

A current density of 76×10^{6} A/m^{2} gives an applied field of 2 T at $r=0$, $z=0$. The resulting field distribution near the AMR is relatively uniform compared to most of the domain, but some curvature in the flux lines is evident.

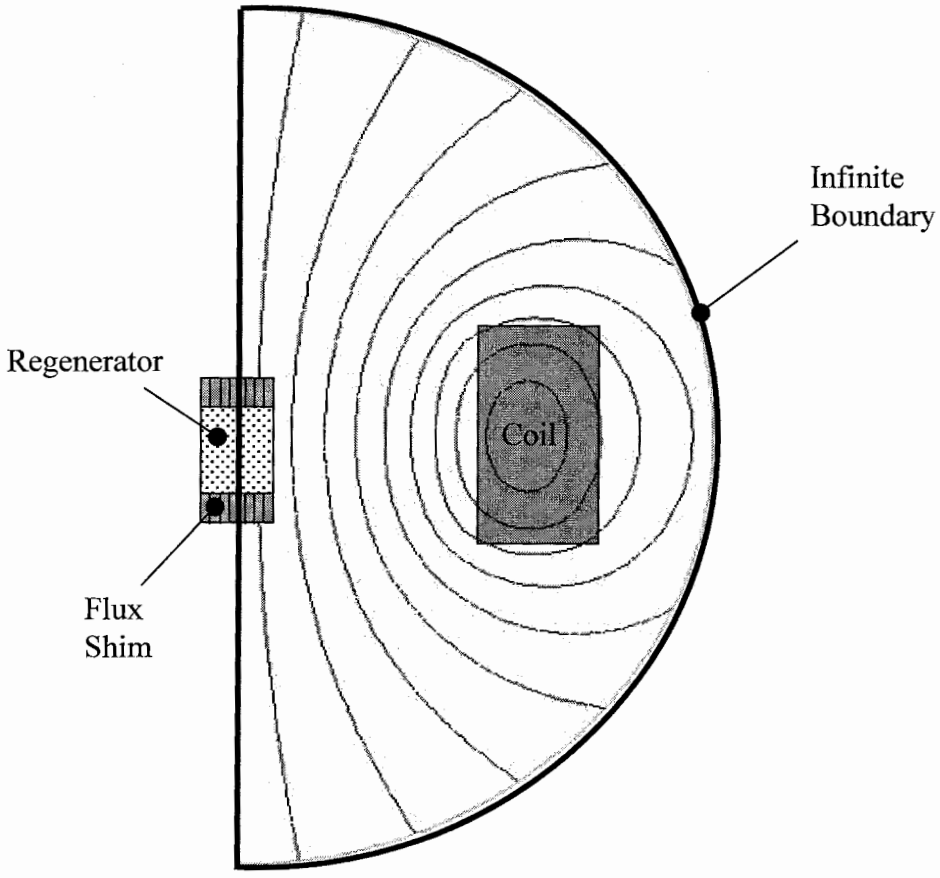

Figure 4.9: Realistic domain.

4.4.1 Numerical Results for Realistic Field

Figure 4.10 shows the relative magnetization for an AMR bed without flux shims. The regenerator bed radius is 12.5 mm and the regenerator length is 25 mm. The applied field is 2 T and the bottom of the regenerator is at 285 K while the top part is at 302 K. The plot shows the relative magnetization decreases near the boundaries.

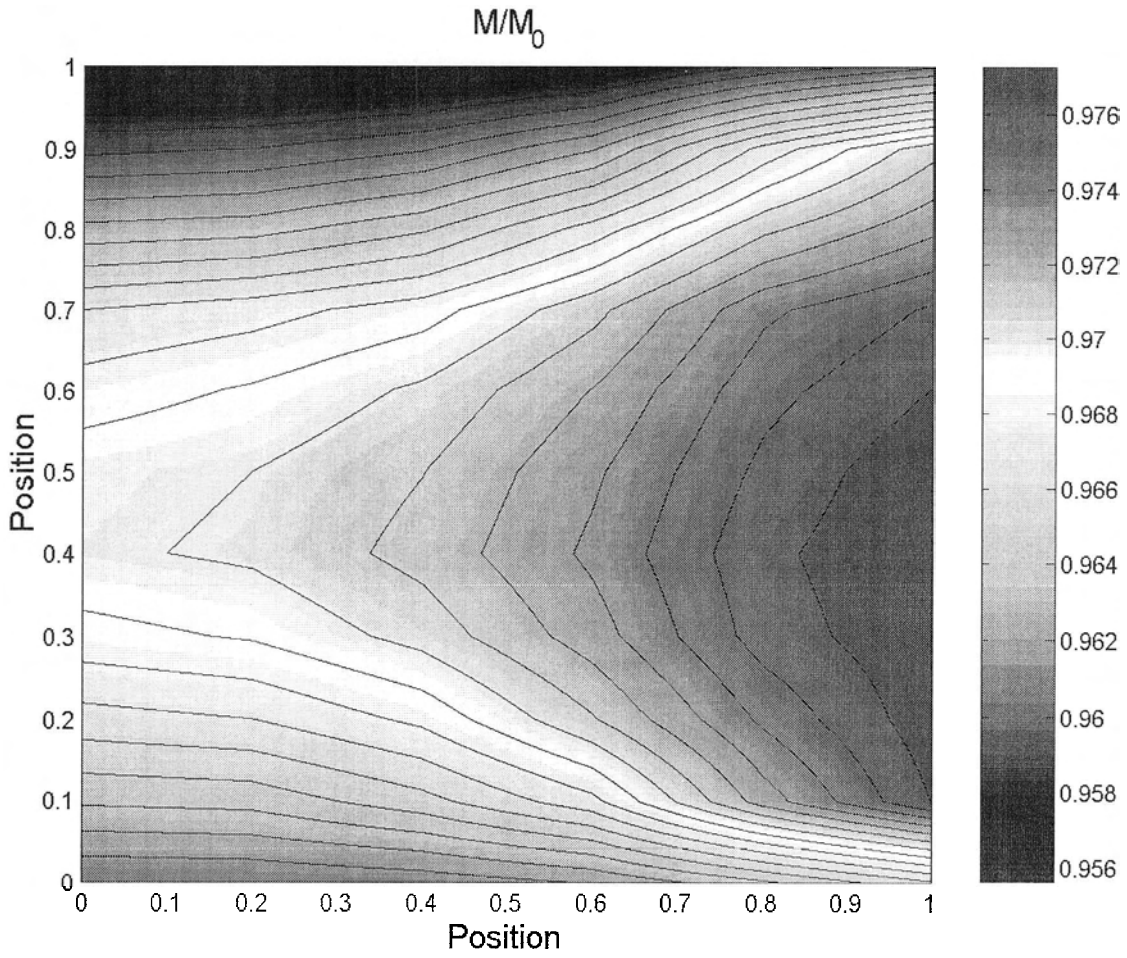

Figure 4.10: Two-dimensional plot of the regenerator bed with 25 mm length.

The cold end of the AMR is positioned at the bottom of the figure and behaves ferromagnetic while the hot end is located at the top of the figure and behaves as a paramagnetic. From the figure it can be seen that the relative magnetization is below 1 at each location in the regenerator bed and as expected the sections that are paramagnetic show a larger response to demagnetizing fields.

Figure 4.11 shows the relative magnetization along the center and for different radii of the AMR. In the figure *r=0* represents the center of the bed while *r=1* is the outside diameter.

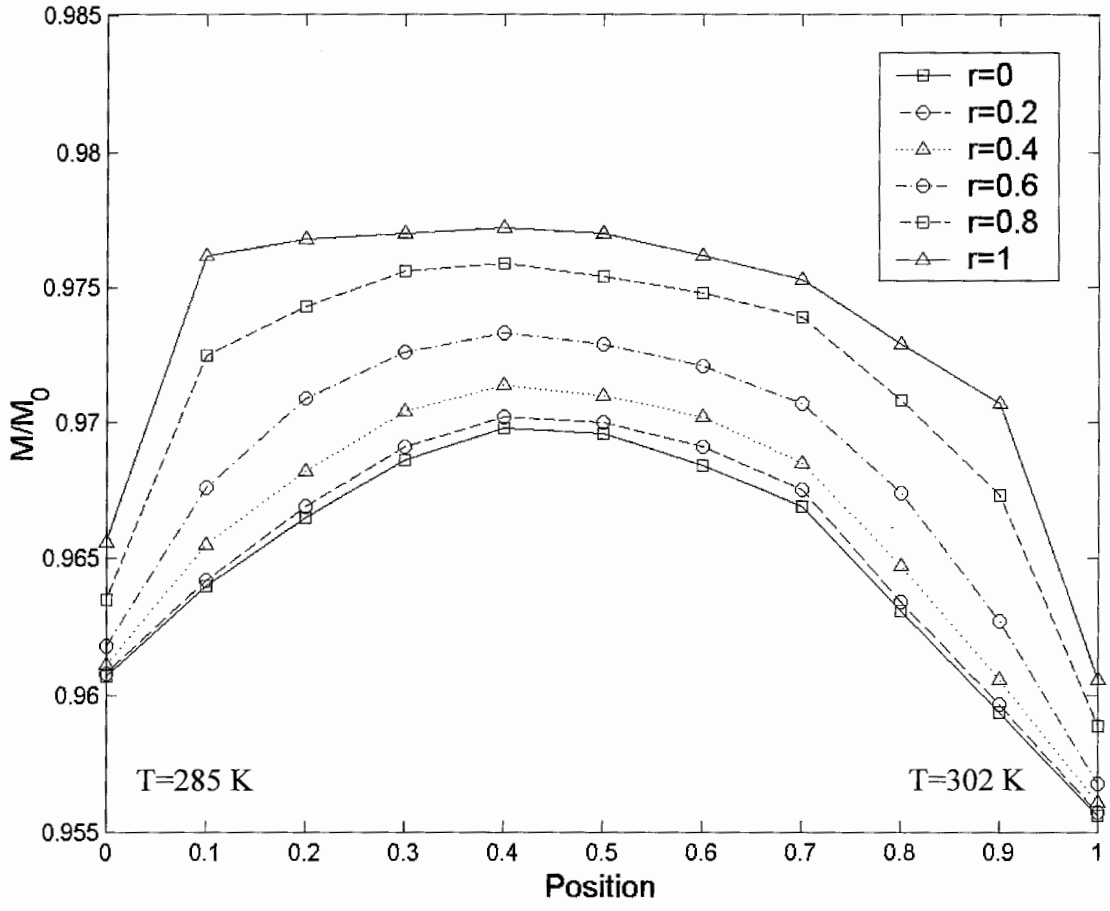

Figure 4.11: Relative magnetization of 25 mm regenerator at various radiuses.

From the figure it can be seen that the demagnetization effect is higher at the center of the bed (*r=0*) than the outer radius of the AMR (*r=1*). Also the sections that are paramagnetic show a larger response to demagnetizing fields.

When the flux shims are added on both sides of the regenerator, a decrease in demagnetization is expected. For this purpose another simulation is run with iron pieces. Again the applied field is set to 2 T and the regenerator bed length is chosen to be 25 mm. The bottom of the bed is 285 K and the top part is 302 K. The result is shown in Figure 4.12.

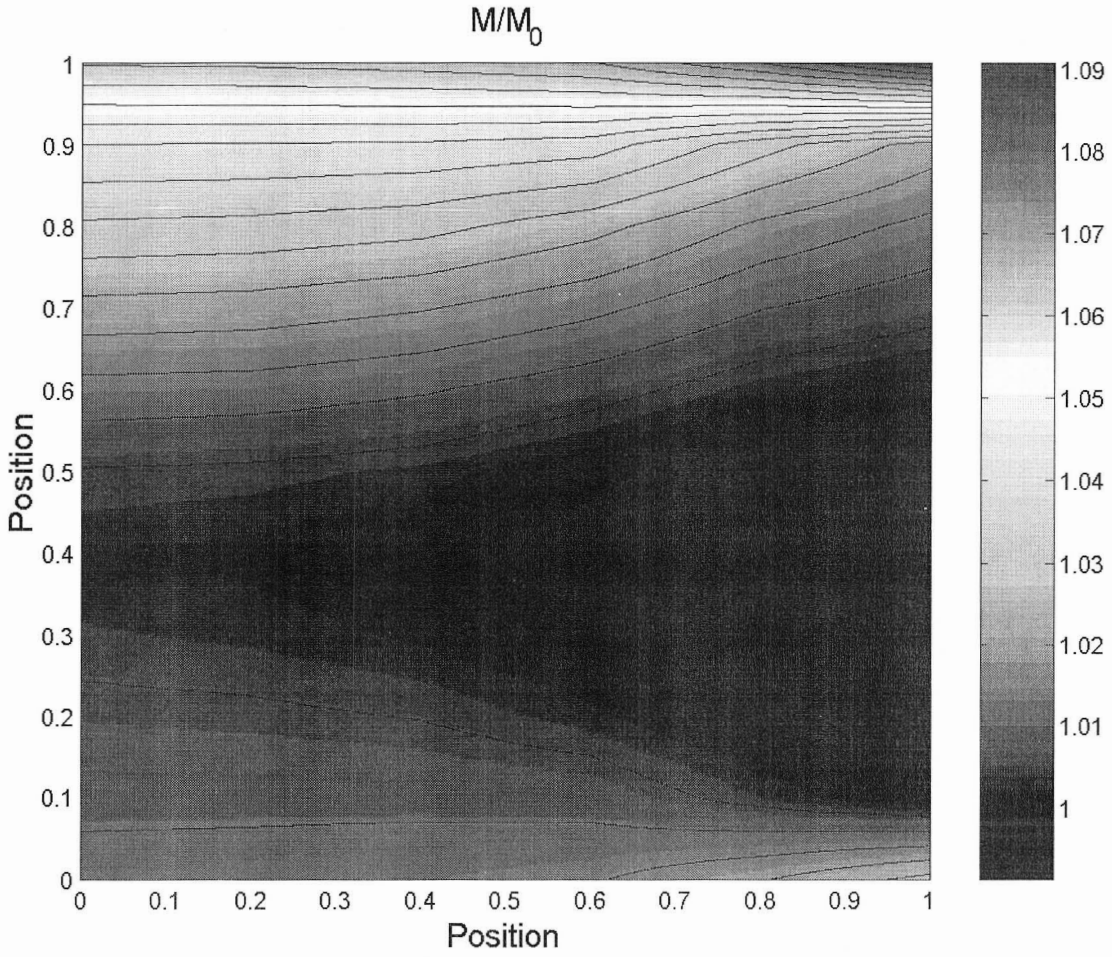

Figure 4.12: Two-dimensional plot of the regenerator bed with flux shims.

From the figure it can be seen that flux shims increase the relative magnetization particularly at the ends of the bed. Because of flux shims the demagnetization fields are canceled and a significant increase is obtained in relative magnetization on both sides of

the AMR. The increase in magnetization at the hot end (paramagnetic) is higher than the cold end of the regenerator bed (ferromagnetic).

The impacts of using the flux shims are shown in Figure 4.13. The results represent the relative magnetization along the center and for different radii of the AMR with flux shims. In the figure *r=0* represents the center of the bed and *r=1* the end.

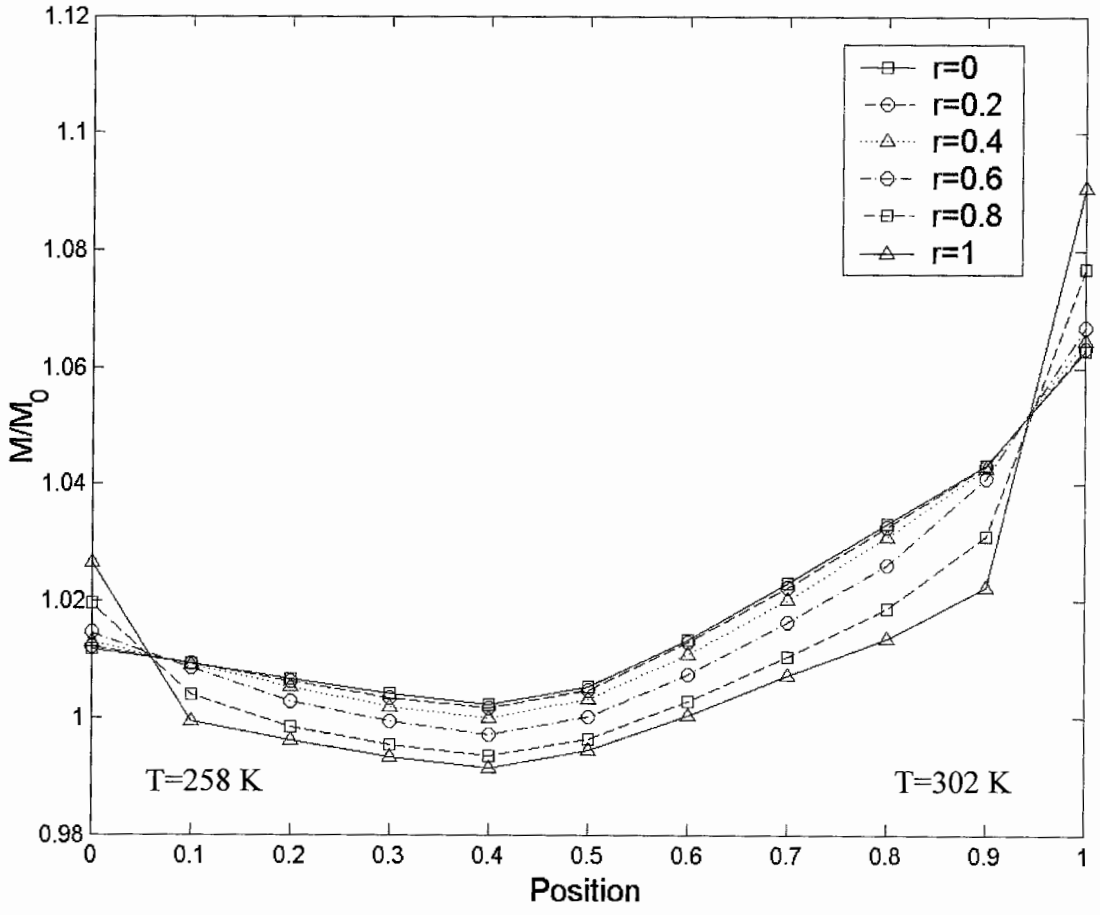

Figure 4.13: Relative magnetization of 25 mm regenerator at various radiuses with flux shims.

The results indicate that the shims reduce the demagnetizing effects through the AMR. The increase in magnetization is more significant along the center of the bed compared to the end. Also the magnetization is higher for the material that is near and above the Curie temperature.

Chapter 5

Conclusions and Recommendations

5.1 Conclusions

Magnetic refrigeration relies on the ability of a magnetic substance to undergo a significant change in entropy due to the application or removal of an applied field. In Active Magnetic Regenerators the working material tends to operate near the magnetic ordering temperature, and, because the AMR creates a temperature gradient through the bed, the local magnetic permeability can vary widely. Due to geometry and non-uniform material properties, an AMR bed is subject to non-negligible demagnetizing effects that can reduce the entropy change due to an applied field as compared to that of a long-thin specimen.

A numerical investigation of demagnetizing effects in AMRs was performed at various regenerator lengths and temperatures. Model results for single-material beds show the impacts of temperature and regenerator lengths on effective magnetization and suggest that demagnetization effects will reduce the magnetic work performed at each location in the AMR. A solution to this problem is proposed. From results, the following conclusions can be made:

- Results with a fixed length and with uniform but varying temperatures show that as the temperature of the regenerator bed goes from a point below the Curie temperature to a temperature greater than the Curie point, the relative magnetization decreases. Therefore, an AMR operating near or above the phase transition region will not perform as much as work as expected and will be less effective in pumping heat.

- As expected, the impact of demagnetization in AMRs at uniform temperature depends on the aspect ratio of the regenerator. Long regenerators with small diameter have higher magnetization through the AMR. Thus, regenerators with higher aspect ratios are preferable.

- When the magnetic refrigerant is operating in an AMR cycle, the temperature gradient across the bed creates a strong variation in magnetization as a function of position. The ends of the AMR experience the greatest reduction in magnetization due to the demagnetization field.

- To counteract the demagnetization effect, the use of soft ferromagnetic material on either end of the AMR was modeled. The use of passive flux shims shows that the demagnetization effect can be counteracted when the applied field is 2 T and that the effective magnetization change can be enhanced.

5.2 Recommendations for Further Work

There are a number of areas where additional research is required to completely investigate demagnetization effect in AMRs. The following list identifies areas that require further work:

a. Numerical results should be combined with experimental results. Several experiments will be run in order to understand better the effects of demagnetization fields in regenerator beds.

b. The results shown in this thesis are for Gadolinium only. Other rare-earth elements such as, Terbium and Erbium should be investigated. In a multi-layered bed, one of the layers may be operating below its Curie temperature (being ferromagnetic) and, thereby, acting like a flux shim on an adjacent material that is above its Curie point (paramagnetic).

c. In an AMR of finite size, the demagnetizing effect depends upon operating conditions. Geometry is not the only concern. AMR materials tend to operate around their magnetic ordering temperature where magnetization is a strong function of both temperature and applied field. For low field operation (<2 T), demagnetizing effects are expected to be more significant than for higher fields (>5 T). However, since second order magnetic materials operate near the transition temperature the material will not be saturated. Thus, even for high field operation, demagnetization fields may be a concern. Therefore, more

investigation is required for demagnetization in regenerator beds at higher applied fields (0.1 T,..,5.0 T).

d. In simulations, the magnetic properties of 1018 steel were used for flux shimming. Higher relative magnetization may be obtained by using other magnetic materials.

Appendix A

Flux Shim

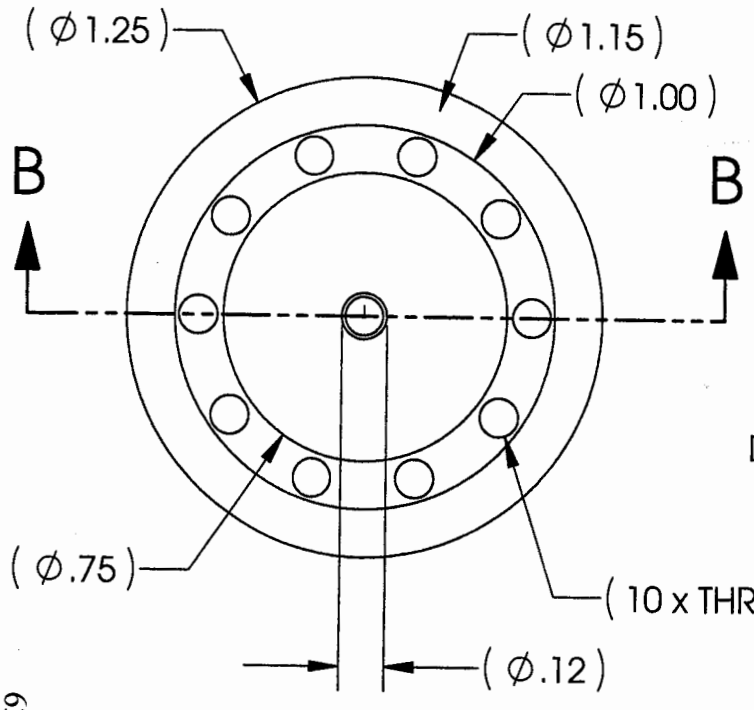

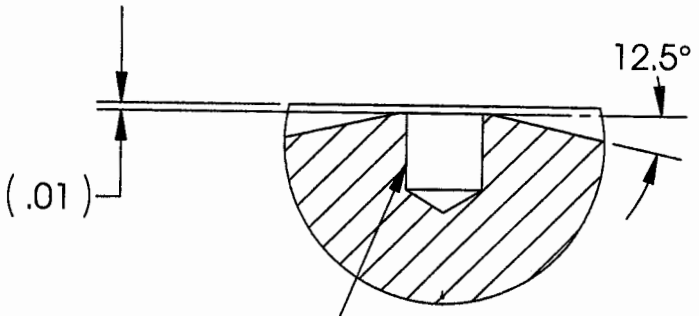

DRILL 0.1" DEEP AND BOTTOM TAP # 4-40

DETAIL F
SCALE 4 : 1

63

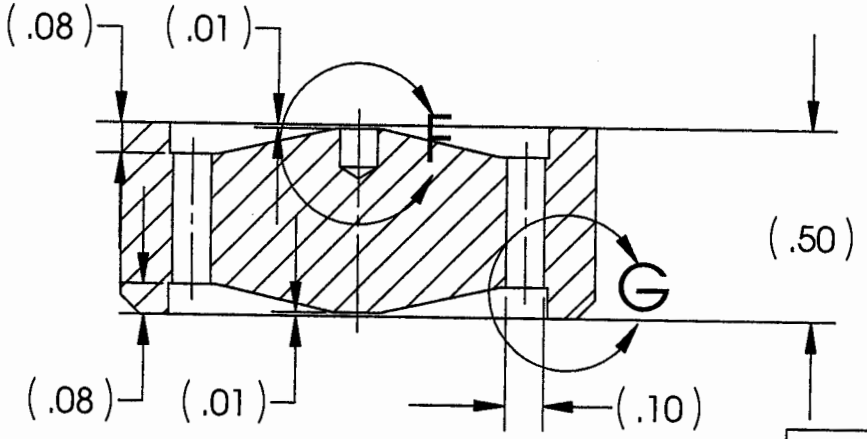

SECTION B-B

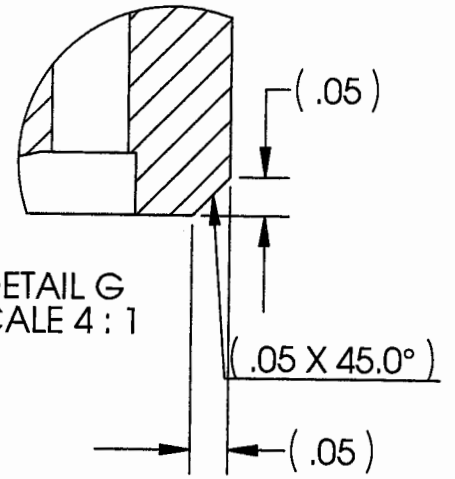

DETAIL G
SCALE 4 : 1

NEXT ASSY	USED ON
APPLICATION	

DIMENSIONS ARE IN INCHES
TOLERANCES:
FRACTIONAL ±
ANGULAR: MACH ± BEND ±
TWO PLACE DECIMAL ±0.010
THREE PLACE DECIMAL ±0.001

MATERIAL 1018 STEEL

FINISH --

	NAME	DATE
DRAWN	Ozan Peksoy	21/July/03
CHECKED		
ENG APPR.		
MFG APPR.		
Q.A.		

COMMENTS:

Quantity: 4

University of Victoria

SIZE	DWG. NO.	REV.
A		
SCALE:2:1	WEIGHT:	SHEET 1 OF 1

References

1. J. Larminie and A. Dicks, "Fuel Cell Systems Explained", John Wiley & Sons Ltd., England, (2003).
2. D. S. Scott, "Smelling Land", Int. J. Hydrogen Energy, Vol. 19, No. 1, (1994), pp. 3-5.
3. D. S. Parasnis, "Magnetism", Science Today Series Harper & Brothers Publishers, New York, (1961).
4. F. R. Fickett and R. B. Goldfarb, "Magnetic Properties of Materials at Low Temperatures", American Society for Metals, (1983).
5. Allan H. Morrish, "The Physical Principles of Magnetism", John Wiley & Sons, Inc., New York, (1965).
6. E. W. Lee, "Magnetism an Introductory Survey", Dover Publications, Inc., New York (1970).
7. B. F. Yu, Q. Gao, B. Zhang, X. Z. Meng and Z. Chen, "Review on Research of Room Temperature Magnetic Refrigeration", International Journal of Refrigeration 26, (2003) pp. 622-636.
8. K. A. Gschneidner, Jr. and V. K. Pecharsky, "Magnetic Refrigeration", Ames Laboratory and Department of Materials Science and Engineering, Iowa State University, Chapter 25, (2000), pp. 522-524
9. A. M. Rowe, M-A. Richard, R. Chahine, T. Bose, "Refrigerator Prototype for Liquefaction of Hydrogen: Active Magnetic Regenerator Development", Institute for Integrated Energy Systems (IESVic), University of Victoria, (2003).

10. Cristopher E. J. Reid, "Development of Magnetic Refrigerants for Active Magnetic Regenerative Refrigerators", M. A. Sc. Thesis, University of Victoria, (1995).

11. A. M. Rowe, "Active Magnetic Regenerators: Performance in the Vicinity of Para-Ferromagnetic Second Order Phase Transitions", Ph. D. Thesis, University of Victoria, (2002).

12. Richard L. Coren, "Basic Engineering Electromagnetics", Prentice-Hall, Inc., New Jersey, (1989).

13. S. Yu. Dankov, A. M. Tishin, V. K. Pecharsky and K. A. Gschneidner, Jr., "Magnetic Phase Transitions and The Magnetothermal Properties of Gadolinium", Physical Review B, 57:6, (1998), pp. 3478-3490.

14. A. Bejan, "Convection Heat Transfer", John Wiley and Sons, Inc., New York, (1984).

15. D. Jiles, "Introduction to Magnetism and Magnetic Materials", Chapman and Hall, New York, (1991).

16. Caudle, K. J., "Characterization of Regenerator Geometries", M. A. Sc. Thesis, University of Victoria, (1997).

17. Daryl L. Logan, "A First Course in the Finite Element Method", Brooks/Cole, Pacific Grove, (2002).

18. J. A. Barclay, "Prospects for Magnetic Liquefaction of Hydrogen", 18th. International Congress of Refrigeration, Montreal, (1991), pp. 297-301.

19. A. M. Rowe and J. A. Barclay, "Ideal Magnetocaloric Effect for Active Magnetic Regenerators", Journal of Applied Physics, Vol. 93, No. 3, (2003), pp. 1672-1676.

20. J. A. Brug and W. P. Wolf, "Demagnetizing Fields in Magnetic Measurements. I. Thin Discs", American Institute of Physics, (1985), pp. 4685-4694.

21. J. A. Brug and W. P. Wolf, "Demagnetizing Fields in Magnetic Measurements. II. Bulk and Surface Imperfections", American Institute of Physics, (1985), pp. 4695-4701.

22. Du-Xing Chen, J. A. Brug, R. B. Goldfarb, "Demagnetizing Factors for Cylinders", IEEE Transactions on Magnetics, Vol. 27, (1991), pp. 3601-3619.

23. A. J. DeGregoria, "Modeling The Active Magnetic Regenerator", Advances in Cryogenic Engineering, Vol. 37, Part B, (1992), pp. 867-873.

24. A. M. Tishin and Y. I. Spichkin, "Magnetocaloric Effect at The Field-Induced First Order Transition In Rare Earth Metals and Alloys".

25. G. Green, J. Chafe, J. Stevens and J. Humphery, "A Gadolinium-Terbium Active Regenerator, Advances in Cryogenic Engineering", Vol. 35, (1990), pp. 1165-1174.

26. W. Dai, B. G. Shen, D. X. Li, Z. X. Gao, "Application of High-energy Nd-Fe-B Magnets in the Magnetic Refrigeration", Journal of Magnetic Materials 218, (2000), pp. 25-30.

27. Warburg, E., Ann. Phys. Chem., 13, (1881), p. 141.

28. A. M. Rowe, O. Peksoy and J. Barclay, "Demagnetizing Effects in Active Magnetic Regenerators", Accepted for publication in Advance in Cryogenic Engineering, Vol. 47.

29. A. Rowe, M-A. Richard, A. Tura, R. Chahine and J. Barclay, "An Overview of Operating Experience Using The AMR Test Apparatus", Accepted for publication in Advance in Cryogenic Engineering, Vol. 47.

30. K. A. Gschneidner, Jr. and V. K. Pecharsky, "The Influence of Magnetic Field On The Thermal Properties of Solids", Ames Laboratory and Department of Materials Science and Engineering, Iowa State University, A287, (2000), pp. 301-310.

31. Q. Chen, "A Review of Finite Element Open Boundary Techniques for Static and Quasi-Static Electromagnetic Field Problems", IEEE Transactions On Magnetics, Vol. 33, No. 1, (1997), pp. 663-676.

32. V. K. Pecharsky, K. A. Gschneidner Jr., "Magnetocaloric Effect and Magnetic Refrigeration", Journal of Magnetism and Magnetic Materials 200, (1999), pp. 44-56.

33. L. Zhang, S. A. Sherif, A. J. DeGregoria, C. B. Zimm and T. N. Veziroglu, "Design Optimization of a 0.1-ton/day Active Magnetic Regenerative Hydrogen Liquefier", Cryogenics 40, (2000), pp. 269-278.

34. J. B. M. Melissen, "A New Coordinate Transform for The Finite Element Solution of Axisymmetric Problems In Magnetostatics", IEEE Transactions On Magnetics, Vol. 26, No. 2, (1990), pp. 391-394.

35. Richard M-A., Rowe A. M., Chahine R., Bose T. K. and Barclay J. A., "Towards Magnetic Liquefaction of Hydrogen: Experiments With an Active Magnetic Regenerator Test Apparatus", presented at the Canadian Hydrogen and Fuel Cell Conference, Vancouver, CANADA, (2003).

36. Yi Zhuo, Chahine R. and Bose T. K., "Magnetic Entropy Change in The Ge-rich alloys Gd-Si-Ge", Magnetics, Vol. 39, No. 5, (2003), pp. 3358-3360.

37. M. Foldeaki, R. Chahine, B. R. Gopal, T. K. Bose, X. Y. Liu and J. A. Barclay, "Effect of Sample Presentation On The Magnetic And Magnetocaloric Properties of Amorphous $Gd_{70}Ni_{30}$", Journal of Applied Physics, Vol. 83, No. 5, (1998), pp. 2727-2734.

38. Ansys 6.1, Software Package, Electromagnetics.